

Modelling the effects of climate change on urban coastal-fluvial flooding

Short title: Climate change effects on urban flooding

Jennifer Isabel Munro Kirkpatrick¹, Agnieszka Indiana Olbert¹

College of Engineering and Informatics, Ryan Institute, National University of Ireland Galway, University Rd., Galway, Ireland

Emails: indiana.olbert@nuigalway.ie; jenny.kirkpatrick@outlook.com

Corresponding author: indiana.olbert@nuigalway.ie

Abstract

In coastal floodplains, high river flows and high coastal water levels can result in extensive flooding. Twenty-first century climate change is expected to alter these flood mechanisms. In this study, a coastal city of Cork, Ireland is used as a case study to investigate changes in flood mechanisms, dynamics and extents due to climate change. A hydrodynamic flood model MSN_Flood was used to compute potential future inundation patterns for a range of climate scenarios based on estimates of current, medium-range and high-end projections of extreme river flows and sea levels.

Results illustrate that the flood mechanism is critical in controlling patterns and extent of inundation. Peak river discharges are the primary contributor to extreme flood events under the current climate scenario, however, high-end climate change could result in coastal inundation of comparable magnitude. The most extreme flood events affect the entire city centre - occurring as a result of a combination of fluvial and coastal drivers. The interaction of extreme fluvial discharges and coastal water levels is complex and characterised through comparison of multiple scenarios. This research establishes a best practice methodology for assessment of urban coastal-fluvial flood risk under a changing climate and can be used to determine climate-resilient flood management measures.

KEY WORDS: Climate Change; Coastal flooding; Fluvial flooding; Hydrodynamic modelling; Nested model; Urban flooding;

1 INTRODUCTION

Flooding is the most frequent and hazardous of all natural disasters (ICHARM 2009), with the most extreme flooding generally occurring in estuaries as a result of a combination of high river flows and high coastal water levels. Globally, many urban areas have been developed in coastal plains along the banks of large rivers, and these are subject to flooding due to both fluvial and coastal drivers. The most severe coastal floods are those driven by a combination of high river discharges, astronomical tides, storm surges and/or waves acting simultaneously.

Extensive research exists demonstrating that flooding has increased in frequency in recent decades (Hall *et al.* 2014; Kundzewicz 2012), fuelling concern that climate change is influencing flood regimes. Predicted increases in sea level, rainfall and storm winds are likely to escalate the risk of flooding in the future (Purvis *et al.* 2008). This will have significant socio-economic consequences, compounded by the fact that, over recent decades, coastal populations have continued to grow much more rapidly than the global mean population (e.g. McGranahan *et al.* 2007). Currently, over 600 million people worldwide live in along the coast (<10 m elevation) and it is predicted that this number will increase to more than 1 billion by 2050 (Merkens *et al.* 2016). Human activities in coastal regions, including land reclamation and infrastructure development, also alter the natural behaviour of the coastal zone and impact on the nature of flooding.

With projected changes in climate and predicted increases in coastal development (associated with upwardly trending coastal populations), it is envisaged that flood risk and associated costs will increase in the future. The average annual cost of flood damage in coastal cities is projected to rise globally from US\$6 billion in 2005 to US\$1 trillion by 2050, under present protection levels (Hallegate *et al.* 2013). Taking into account an infrastructure-based adaptation, the global annual flood losses are still projected to exceed US\$60 billion by 2050. Consequently, an in-depth understanding of flood mechanisms and the effects of climate change will provide a significant support for the decision making in flood defence design and flood risk management.

Coastal-fluvial flooding is complex as it results from a combination of interacting drivers, such as stochastic meteorological conditions and deterministic local sea levels. Additionally, the already hydraulically complicated hydrodynamics of natural floodplains is exacerbated by complex urban developments. These generally consist of dense street networks and extensive buildings, which control the routing of water across the floodplain. Even if flood flow patterns are well understood for the current climate, flood characteristics are likely to alter in future in response to climate change, continuing urbanisation and flood defence adaptation. These changes may affect not only flood water levels and associated flood extents but also the pattern of inundation due to a shift in flood mechanisms. Understanding hydraulic conditions on existing floodplains is not trivial, and projecting into the future is extremely difficult. However, when the mechanisms of flooding are identified for a particular floodplain and potential climate-driven changes estimated, the impact of future river discharges and coastal water levels can be determined using flood inundation models. Currently, the most common models utilised in flood assessments are hydrodynamic models, which solve equations of fluid motion (Teng *et al.* 2017). These are particularly useful as boundary conditions can be modified to investigate inundation in response to different future scenarios.

Hydrodynamic modelling can provide an assessment of the degree of flooding and related impacts in response to particular flood mechanisms, and so be utilised to reduce and manage flood risk (Parry et

al. 2009). This is essential as changes in inundation do not necessarily exhibit a linear relationship with changes in water volumes (Veijalainen *et al.* 2010). Accurate modelling of complex coastal-fluvial flood dynamics and interactions within these combined systems is critical for realistic simulation of inundation. Recent developments in hydrodynamic modelling, such as multi-scale model nesting and advances in computational resources through numerical domain decomposition and multi-core architecture, allow us finally to treat the model domain as a multi-scale problem and provide accurate solutions at various scales, ranging from coastal sea or estuary scale down to the dense street network of the inundated urban area (e.g. Barnard *et al.* 2019; O'Neill *et al.* 2018).

In this context, the primary objective of this paper is to provide a methodology for comprehensive forecasting and assessment of urban flooding in consideration of climate change. The methodology is illustrated with a case study of Cork Harbour, for which a numerical model is used to investigate (1) conditions under which coastal-fluvial flooding may occur under current and future climate, and (2) potential effects of climate change on shifts in pattern and impact of coastal and fluvial mechanisms. This study builds on previous work (Comer *et al.* 2017; Olbert *et al.* 2017) to extend our understanding of flood regimes in the current climate to possible future climate scenarios. The development and implementation of techniques that enhance confidence in projections of change in flooding are essential to aid climate adaptation decisions and facilitate effective foreshore management.

In this paper, high-resolution grid scale modelling of a dense urban area under various projected climate scenarios has been conducted and various combinations of extreme floods analysed. The urban area of Cork City, Ireland – frequently subject to coastal and fluvial flooding – was used to investigate changes in flood mechanisms, dynamics and extents due to climate change. Extensive fluvial-coastal flooding of Cork City in November 2009, resulting in damage of over €100 million, prompted the current investigation. A state-of-the-art multi-scale nested hydrodynamic flood model (MSN_Flood) is utilised herein to investigate flooding in Cork, and a range of future climatic conditions for different flood drivers employed to provide a comprehensive forecast of potential future flood scenarios. The MSN_Flood model has been successfully used in recently completed flood research for Cork City and was found capable of resolving the complex hydrodynamics of Cork floodplains (Comer *et al.* 2017; Olbert *et al.* 2017).

2 CORK CITY FLOODING

Cork's low average elevation and extensive coastline make the city especially susceptible to coastal hazards. With sea level rise and project climate change the flood risk is likely to increase significantly.

2.1 Study area

Cork City is situated on the mouth of the River Lee, on the South-West coast of Ireland (Figure 1). The Lee drains an area of approximately 1,253 square kilometres (km²) (Appendix A, Figure A.1) and discharges to Cork Harbour, a 350 km² tidal estuary feeding to the the Celtic Sea and wider North-East (NE) Atlantic. The river is approximately 115 km long and is sourced in the Shehy Mountains on the western border of County Cork. The Electricity Supply Board (ESB) operates two hydro-electric dams on this river, forming the Innishcarra and Carrigadrohid reservoirs, approximately 13 km and 27 km west of Cork City respectively. These provide up to 35x10⁶ cubic metres (m³) of storage, and controlled

discharge, of floodwaters (Halcrow 2014). Discharges from these dams, combined with inflows from the downstream Shournagh, Bride and Curragheen tributaries, control the water volumes entering Cork City. Seawater intrusion from Cork Harbour also influences fluvial water levels in the River Lee, although this is constrained by the waterworks weir approximately 8 km upstream of the harbour.

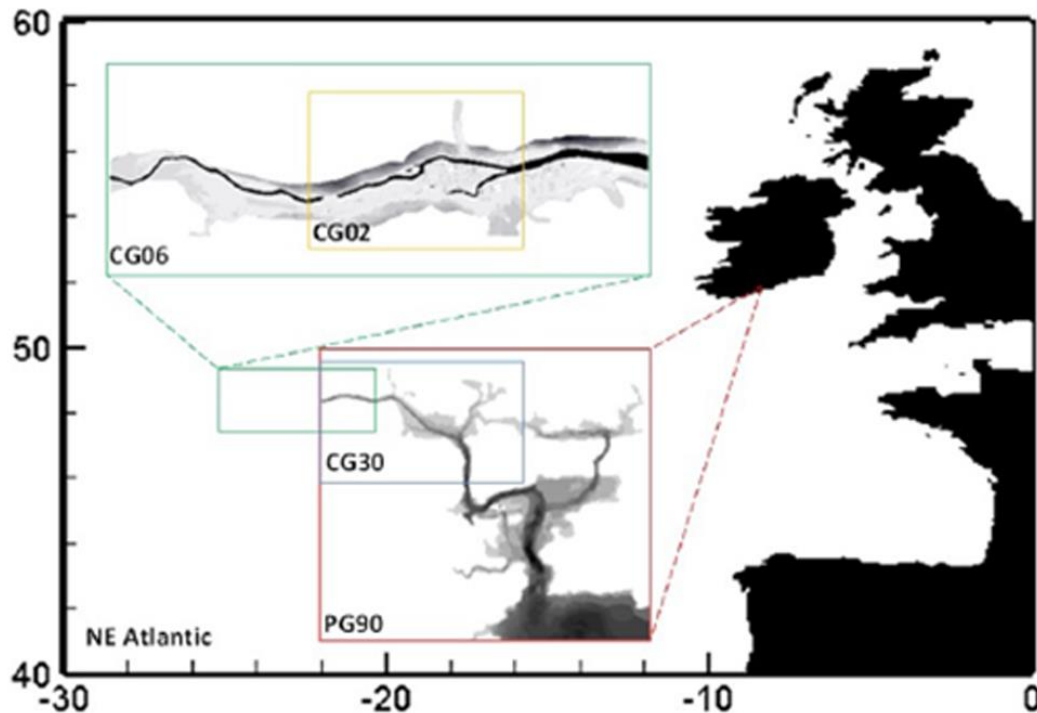


Figure 1: Study area, with four-level nesting structure of Cork Harbour and Cork City nested models (after Comer, et al., 2017)

2.2 Flood mechanisms and climate change

Increases in mean temperatures and rising global sea levels are projected for the 21st Century by the Intergovernmental Panel on Climate Change (IPCC) Fifth Assessment Report (IPCC 2013). Elevated temperatures increase the amount of water vapour in the atmosphere, thereby increasing mean precipitation and the frequency of extreme precipitation events. Alongside elevated sea levels, these patterns of change are likely to exacerbate flooding in North-Western Europe (Lehner *et al.* 2006; Murphy & Charlton 2008). However, the exact impact on flood mechanisms, particularly on a catchment scale, is difficult to ascertain.

2.2.1 Fluvial flood mechanisms

Fluvial flooding is generally caused by intense or prolonged precipitation, associated flood waters are controlled not only by the nature of the precipitation event but also by catchment characteristics and antecedent weather conditions. In Ireland, climate change is expected to alter evaporation and precipitation patterns and so significantly affect the hydrological cycle (Murphy 2013). Temperatures are projected to increase by up to 2.9°C (Joint Research Centre 2014), with winters becoming wetter and summers drier (Dunne *et al.* 2008). However, there is substantial uncertainty in estimates of climate change impacts on peak fluvial flows (Bastola *et al.* 2011a). A number of different studies have assessed these impacts for Irish catchments for the 21st Century, using a range of different climate

models, emission scenarios and hydrological models, and these are summarised in Table 1. Although no studies were identified relating directly to the Lee Catchment, research does exist encompassing the Blackwater and Bandon Catchments, immediately north and south of the Lee (e.g. Bastola *et al.* 2011b; Steele-Dunne *et al.* 2007). These consistently predict an increase in peak flows, largely due to projected increases in winter precipitation and in extreme events. However, the magnitude of change varies between catchments and simulations, with greater uncertainty associated with larger flood events (Bastola *et al.* 2011b).

2.2.2 Coastal flood mechanisms

Along the majority of northern European coasts, mean sea level rise (SLR) is projected to be the main driver of change in coastal flooding, enhanced by changes in storm surges and waves (Vousdoukas *et al.* 2017). Identified projections of future changes in coastal flood mechanisms are summarised in Table 1, for different possible future climate scenarios. This includes potential changes in MSL, land elevation, tidal amplitude and maximum surge height.

Eustatic SLR is expected to continue throughout the coming century due to increasing global temperatures and an associated influx of meltwater from glaciers and ice sheets (Fettweis *et al.* 2013; Levermann *et al.* 2014; Marzeion *et al.* 2012). This has the potential to be enhanced by steric SLR caused by increasing global average sea surface temperature (SST), driving salinity variations and thermal expansion of the oceans (Olbert *et al.* 2012). Projected SLR for the 21st Century varies depending on the climate model utilised and emissions scenario modelled (Table 1). Notably global SLR will not be uniform, due to the complex interrelationships controlling impacts on a local scale (Olbert *et al.* 2012). However, global projections (IPCC, 2013) are found to be reasonably comparable to projected changes for the Irish coast for mid-range future emissions scenario (Olbert *et al.* 2012). Along the southern coast of Ireland relative sea level rise (RSLR) is also enhanced by land subsidence - driven by ongoing isostatic adjustment (Bradley *et al.* 2009), which commenced following the retreat of the British-Irish Ice Sheet after the Last Glacial Maximum (Chiverrell & Thomas 2010).

Sea level can also be enhanced locally by tides, waves and storm surges. While astronomical tides are expected to remain constant over time, it should be recognised that tidal amplitude can be affected by the bathymetry of the ocean (Green 2010) and so may be altered by SLR (Woodworth 2010). Where SLR floods low-lying land, friction and other shallow water effects can increase tidal dissipation, whilst an increase in overall depth within an ocean basin can alter tidal resonance (Pelling & Matthias Green 2014). Despite this potential, it is generally expected that only excessive SLR (>2.0 m) will impact existing tidal patterns (Pickering *et al.* 2012; Vousdoukas *et al.* 2017) (Table 1).

Ocean waves result from strong winds blowing over adjacent seas (Gill 1982), and extreme wave heights occur in response to intense weather systems. These are expected to be altered by climate change (Gallagher *et al.* 2016), however, as Cork City is sheltered within the extensive Cork Harbour, it is considered that there is a negligible effect of waves on flooding in the study area (Olbert *et al.* 2017).

Storm surges generated by low-pressure systems (cyclones) and/or strong winds (Wells 1997), are of relatively low magnitude in the Celtic Sea and are understood to be generated primarily by low-pressure systems in this region (Olbert & Hartnett 2010). A potential increase in the frequency of low-pressure events (IPCC 2013), combined with projected SLR, which will exacerbate surge peaks, has

resulted in a global concern that climate change will result in an increase in the frequency of occurrence and/or elevation of storm surges (e.g. Brown *et al.* 2010; Wang *et al.* 2008; Woth *et al.* 2006). There is, however, substantial uncertainty in projected climate-driven changes in these systems for the North Atlantic region (IPCC 2013). Research is often contradictory, with some predicting an increase in cyclone intensity and frequency (e.g. Dunne *et al.* 2008; Haarsma *et al.* 2013) and others predicting a decrease (e.g. Eichler *et al.* 2013). A decrease in maximum surge height has been estimated for Cork Harbour (Wang *et al.* 2008) (Table 1), although the same research also projects an increase in the frequency of surges of the magnitude typically associated with coastal flooding. This will potentially increase the probability of a major surge occurring contemporaneously with a high tide, although consideration must also be made of tide-surge interactions (Arns *et al.* 2015; Olbert *et al.* 2013).

2.3 Flood modelling

There have been a number of attempts to model Cork City flooding. As part of the Lee Catchment Flood Risk Management Plan (CFRMP) (Halcrow 2014), a Lower Lee hydraulic model and harbour model were developed to assess current and future inundation in Cork City (Halcrow 2009). However, interdependence between flood drivers can lead to compound effects (e.g. Wahl *et al.* 2015) and modelling individual flood drivers separately can lead to inaccurate characterisation of flooding (Moftakhari *et al.* 2017). More recently, the high-resolution multi-nested MSN_Flood model was applied to coastal-fluvial flooding in Cork City (Comer *et al.* 2017) and the multivariate capabilities of the system found to allow realistic modelling of the compound effects of multiple flood drivers in response to given boundary conditions (Olbert *et al.* 2017). Robust representation of wetting and drying within MSN_Flood results in a geographically unconstrained model, adaptable to model domains of any complexity and to multi-open boundary problems. The ability of this model to accurately simulate flood dynamics and quantify the key attributes associated with flood risk – flood wave heights, speeds, propagation patterns and inundation extent – mean that it is highly suited to predicting flood responses to climate change.

3 MATERIALS AND METHODS

The MSN_Flood coastal-fluvial model set-up for Cork City was used in this research to investigate the potential impacts of 21st Century climate change on flood inundation in this urban hub. The following provides an overview of the model and details the specific model boundary conditions and set-up utilised.

3.1 The multi-scale nested flood model

The MSN_Flood model comprises a cascade of 90, 30, 6 and 2 metre resolution nested grids (Figure 1). The lower River Lee is contained fully within the 6 m child grid (CG06), which includes an embedded 2 m grid (CG02) capable of resolving the complex hydraulics of Cork city centre. The model integrates the continuity and momentum equations in order to simulate water elevations and velocities. Floodwater routing is controlled primarily by slope and structural features within urban floodplains, which is represented by the model bathymetry. This was developed using admiralty chart data, high-resolution resolution Light Detection and Ranging (LiDAR) data and river cross-section data (Comer *et*

al. 2017). Full details of the hydrodynamics, nesting structure, calibration and performance of the model are available in Comer *et al.* (2017). Some critical features of the model include the wetting and drying routine, computational efficiency, and accuracy of simulated water elevations and velocity fields – as tested in Olbert *et al.* (2017). These characteristics make the model particularly applicable to this study.

3.2 Boundary conditions

This research utilised the CG06 child grid of the MSN_Flood model, and required determination of fluvial discharges and coastal water levels at the western and eastern model boundaries. Due to the computational power required for the high-resolution CG02, this embedded domain was neglected and city centre inundation was resolved purely by the 6 m domain. In order to consider future flood conditions it is important to understand historic flood events, as these set projected changes in an appropriate context. Knowledge of both historic and potential future extremes is necessary to determine changes in flood regimes. The model was initially run for a variety of scenarios under present climatic conditions; this provided a basis for the quantification of impacts of climate change. In order to model inundation in response to each flood mechanism individually, as well as in response to combined flood mechanisms, it was necessary to determine both average and peak fluvial discharges and coastal water levels.

3.2.1 CG06 western fluvial boundary

The western boundary of the CG06 model domain commences at lower Leemount, immediately downstream of the Shournagh tributary on the River Lee (Appendix A, Figure A.1). Fluvial inflows to the model domain are largely controlled by discharges from the Inniscarra Dam, as well as the Shournagh tributary. Design return periods in hydrology are determined based on an evaluation of the costs involved with a flood event of a given return period, and with adapting to manage the same flood event (Fortunato & Mazzola 2014). For urban drainage, these typically range from 50 to 100 years. This research considered the influence of climate change on a 100-year return period fluvial flood event.

The Office of Public Works (OPW) Flood Studies Update (FSU) Portal provides improved methods of flood estimation in both gauged and ungauged catchments using flood frequency analysis, and quantification of the relationships between physical catchment descriptors (PCDs), flood magnitudes and hydrograph shape. This was utilised here to produce a hydrograph representative of a 100-year event for the upstream model boundary. Due to a lack of publically available OPW river gauge records at the upstream model boundary the catchment was considered as ungauged and the median annual maximum flood (QMED) determined using regression techniques based on the PCDs of the contributing catchment area – adjusted using records from a comparable gauged catchment (pivot site), chosen based on hydrological similarity.

In this study, QMED was initially estimated based on the PCDs of the contributing area (QMED PCD_{rural} = 164 cubic metres per second m³/s) and adjusted to incorporate the influence of urban infrastructure (QMED PCD_{urban} = 167 m³/s). The site (19031, see Appendix A, Figure A.1) with closest hydrological similarity (1.71) was then used to adjust QMED and a growth factor (1.7) was applied based on frequency analysis using pooled records from hydrologically similar catchments. The growth curve was plotted using a generalized extreme value (GEV) distribution, most suited to ungauged

catchments (Murphy 2014). This provided an adjusted QMED of 286 m³/s and a flow of 512 m³/s associated with a 100-year return period, comparable to flows predicted by Olbert et al. (2015) and to the peak recorded at 19012 during the 2009 flood event (560 m³/s). In reality, flows are strongly dependent on operational procedures at Inniscarra Dam and cannot be accurately projected using flood frequency methods. However, dam operational procedures suggest a maximum discharge of around 550 m³/s, (Halcrow 2014), which is again comparable to the projected peak. This derived value is, therefore, considered acceptable as a representation of peak flows along the western model boundary. The shape of the hydrograph is determined from PCDs and adjusted based on a hydrologically similar pivot site containing a sufficient record of large flood events. A river flow of 75 m³/s is considered a reasonable estimate of model inputs from the River Lee during normal (baseflow) conditions. Figure 14 shows the synthetic curve of river flows used as boundary conditions for current and future climate scenarios.

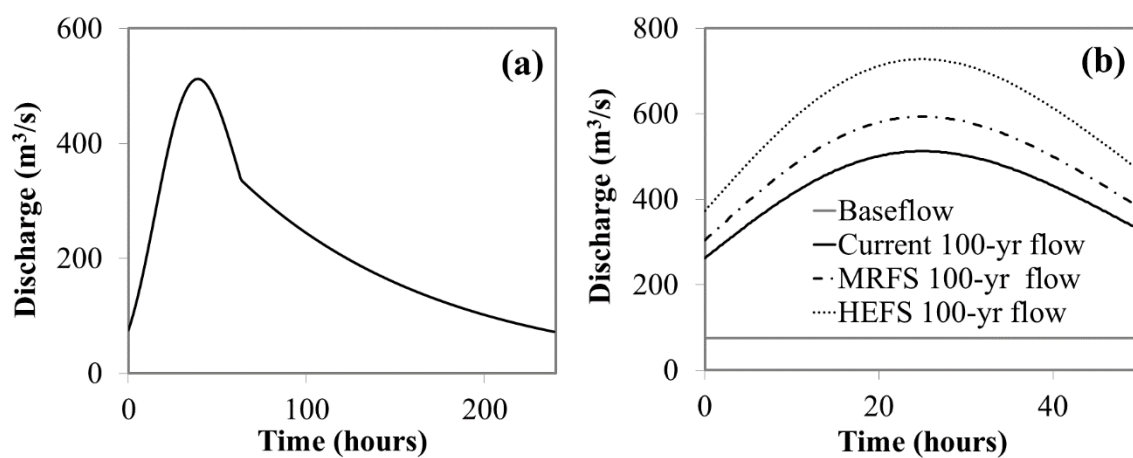


Figure 2: (a) 100-year return period synthetic hydrograph; and (b) extracted model inputs for average and peak flow conditions, under current and future climate scenarios

3.2.2 CG06 eastern coastal boundary

Published mean spring and neap tide ranges are typically 3.6 m and 2.0 m respectively in Cork Harbour (Hewitt & Lees-Spalding 1982). The average of these values was taken as a representative mean tidal range (2.8 m), resulting in a mean high water tide (HWT) of 1.4 m above mean sea level (MSL) (Figure 3a). The declination of the Moon and Sun, and the elliptical nature of the Moon's orbit contribute to a cycle of tide-generating forces of varying strength (Koppel 2007). A maximum high water spring tidal range of 4.53 m above chart datum (CD) has been determined for a 1,000 year return period (Olbert et al. 2013), from which a maximum HWT of 2.23 m above MSL was estimated (Figure 3b).

Olbert, et al. (2013) carried out extreme value analysis of surges based on field records and numerical model outputs for 48 historical surge events. In order to consider the worst case scenario, the maximum surge residual (0.97 m) associated with the largest available return period (1,000 years) was used to represent the impact of surges on tidal signal in this study. Surge peaks in Cork Harbour are associated with the tidal phase between mid-flood and high water (Olbert et al. 2013), with the occurrence of the peak surge on rising as opposed to peak tide causing a significant difference in

inundation extent (Olbert *et al.* 2015). For the purpose of incorporating surge impact on coastal water levels, the peak surge residual was applied as a constant across the entire tidal signal, as illustrated in Figure 3c and d. This allowed consideration of the worst-case scenario. When considering fluvial mechanisms or MSLR impacts individually, it was assumed the surge residual is equal to zero.

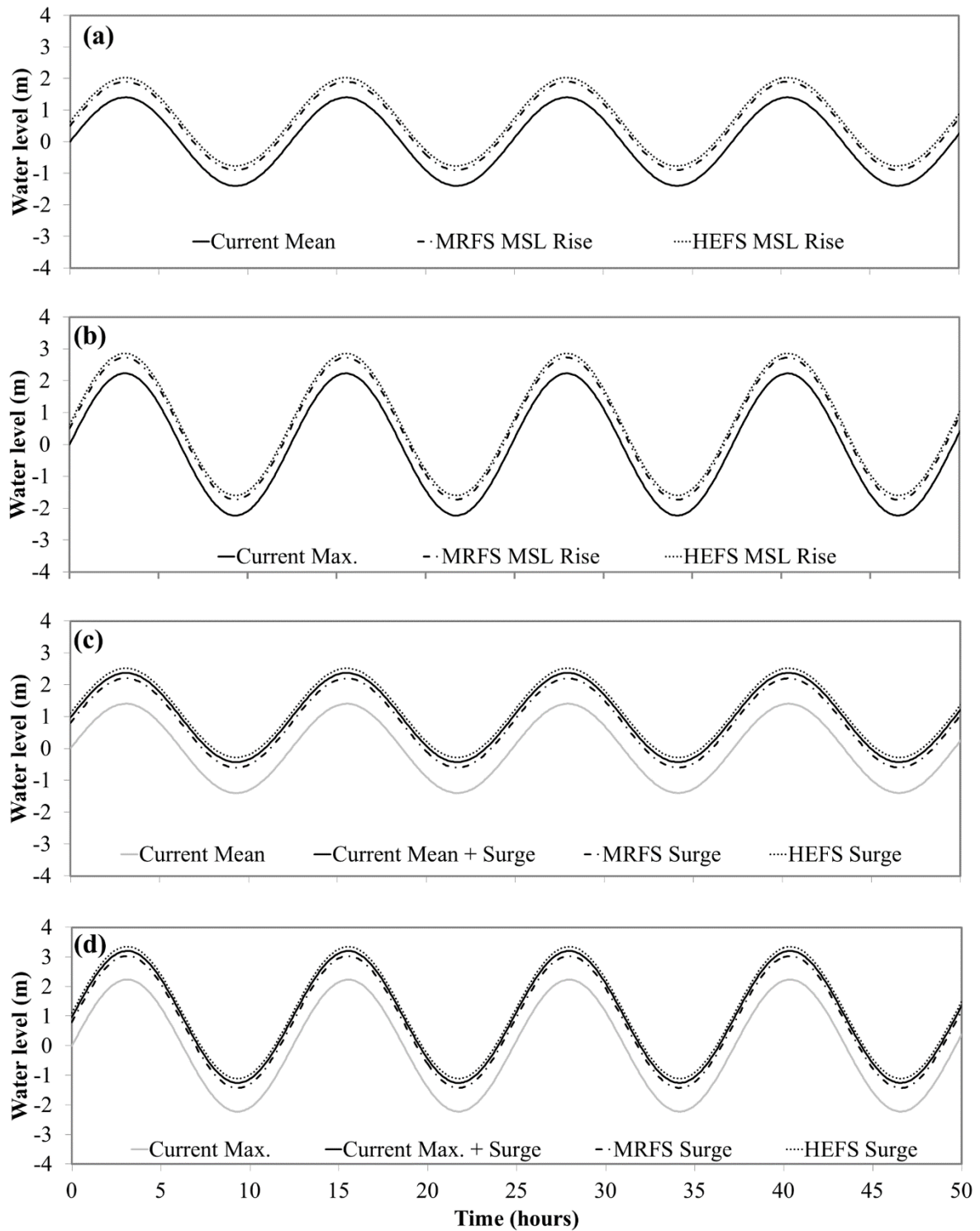


Figure 3: (a) Synthetic mean tidal signals for current, medium range (MRFS) and high-end (HEFS) future scenario mean sea level rise; (b) synthetic maximum tidal signal for current, MRFS and HEFS mean sea level

rise; (c) synthetic mean tidal signal with maximum surge residual for current, MRFS and HEFS surge signals. and (d) synthetic maximum tidal signal with maximum surge residual for current, MRFS and HEFS surge signals.

3.3 Model set-up

Following identification of average and peak fluvial and coastal model inputs for current conditions, the predictions for climate-driven changes in these boundary conditions considered most pertinent for a MRFS and HEFS were applied to peak discharges and water levels based on the collated literature (Table 1). These are summarised in Table 2. A range of model input files were subsequently generated for both present and future climatic conditions (Figure 2b and Figure 3). The model is driven by these boundary conditions and was set-up to compute solutions to the continuity and momentum equations across the model domain at 0.3-second timesteps over a 50-hour duration. Computation time for each model run was 13.4 hours.

4 RESULTS AND DISCUSSION

The model was validated (Section 4.1) and subsequently used to present a range of flood events, for current and potential future climate scenarios (Sections 4.2, 4.3 and 4.4). A total of 96 flood scenarios (eight current and 88 climate-driven future scenarios) were simulated for Cork City, based on estimates of current, MRFS and HEFS extreme river flows and sea levels. These scenarios, and associated maximum areal extent of inundation and volume of floodwater, are detailed in Table 3. Identified runs consider changes to both individual flood mechanisms and combinations of different flood mechanisms.

4.1 Model Validation

Olbert, et al. (2017) calibrated and validated the nested CG06 and CG02 model using flood extent mapping and water level marks from 38 locations in Cork City, collated by the OPW following the November 2009 flood event. The CG06 model alone was utilised here to simulate the 2009 flood and validated against the same observations. The simulation was carried out using boundary conditions defined by water levels recorded in the River Lee and Cork Harbour during the flood event (Figure 4).

A good general spatial match was found between observed flood extent and the CG06 simulation (Figure 5). However, the OPW flood extent polygon is based on a rough field assessment and can be used to provide only a rudimentary assessment of model performance. Additionally, this polygon does not extend across the entire CG06 domain, and so comparisons can be made only of simulated inundation within the vicinity of available data. Marginal differences in simulated and observed extent are detected where data is available, however, these are considered primarily a result of the poorly refined observations rather than inaccuracies within the model. Notably, CG06 was observed to overestimate the extent of flooding in the city centre, with floodwaters extending further east than observations.

Watermarks infer maximum water depth at the time of peak inundation. Time series of water elevations were computed at the locations of watermarks to determine maximum simulated water levels, and a linear regression (Figure 6) illustrates the relationship between maximum modelled and observed water depths. Agreement is good, with the majority of points lying approximately on the 45° line and the coefficient of determination (r^2) tending towards one. There is, however, a tendency towards overestimation of water elevation, correlating with the overestimation of extent.

Minor deviations in spatial extent and water elevation from observed values are likely a result of the coarser resolution of the CG06 model, in comparison to the CG02 model for which roughness coefficients were calibrated (Olbert et al. 2017). The increased propagation of floodwaters into the city centre is expected to be a result of a failure of the 6 m bathymetry to fully resolve the dense street network, and associated constraints on flows within this region. Additionally, the coarser representation of topography affects the gradient of the water surface, which can influence flow dynamics and explain further deviations in depths and propagations patterns. Some small portion of the error ($\sim 0.1\text{m}$ RMSE) may also be attributed to errors in LiDAR data, which served to construct the model bathymetry (Bates 2010). Overall, regardless of deviations, the CG06 flood model was found capable of reproducing the 2009 flood event and considered suitable to utilise as predictive tool for characterising potential future inundation.

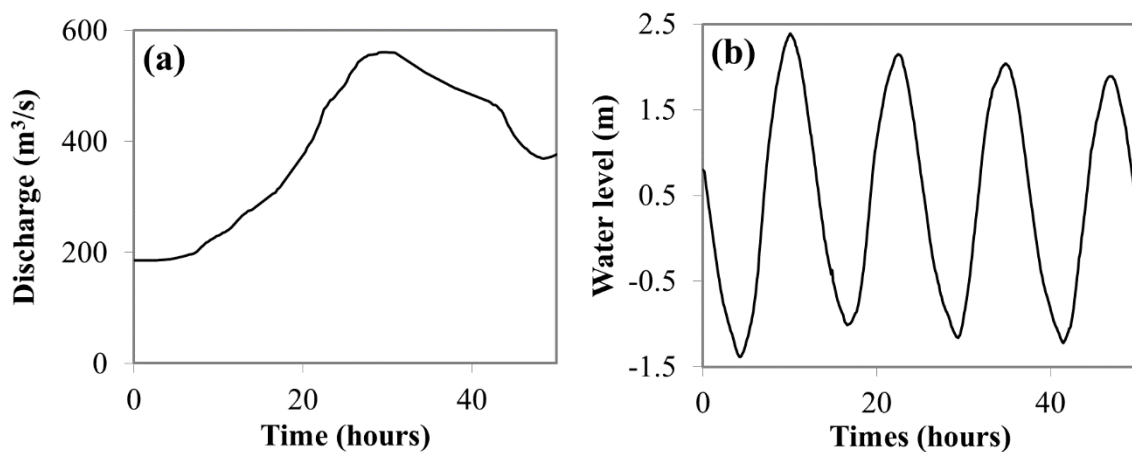


Figure 4: Model boundary conditions for model validation, defined by (a) River Lee flow data (gauge 19011) and (b) tidal water levels (Tivoli tidal gauge) recorded during the November 2009 flood event

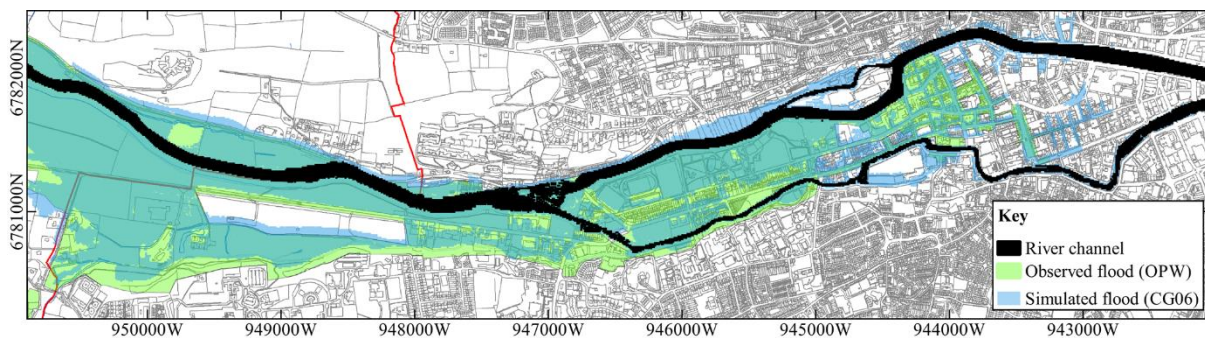


Figure 5: Comparison of OPW post-event mapping and modelled inundation extent for the November 2009 flood event

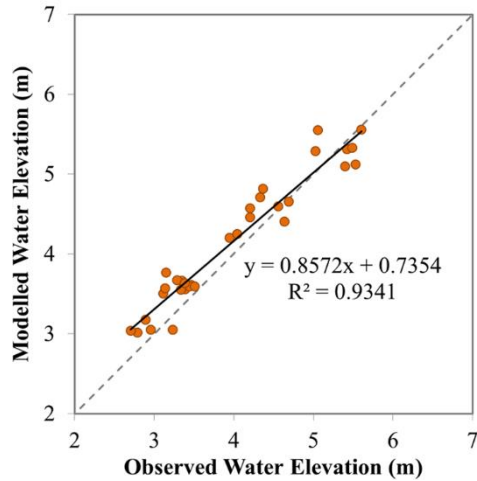


Figure 6: Correlation of modelled and observed water elevations at survey locations

4.2 Fluvial driven flooding

Autonomous modelling of fluvial flooding has shown that fluvial events are the primary contributor to extreme flood events under the current climate scenario (Table 3– C5). The flood wave associated with a 100-year return period discharge affects large areas of rural land to the west of the city before propagating eastwards into suburban areas and channelling through the city street network, causing severe flooding of the western city centre (Figure 7). Climate-driven increases in fluvial flows exacerbate inundation extent, water depths and velocities, with floodwaters extending into the eastern reaches of the city centre for MRFS and HEFS river discharges (Figure 7). Simulation of flooding in response to a MRFS increase in the 100-year return period flow (593 m³/s) results in 208 ha of inundation (Table 3– M21), a 12% increase over the current scenario. Simulation of flooding in response to a HEFS increase in fluvial flows (728 m³/s) results in 242 ha of inundation (Table 3– H21), a 30% increase over the current scenario. Under this scenario, the majority of streets within the city centre are inundated, with only the far eastern reaches of the central island remaining dry.

The maximum water depths associated with fluvial flooding are detailed in Table 4 and illustrated in Appendix A, Figure A. 2; under MRFS and HEFS river discharges water depths increase significantly. Floodwaters are deepest in rural areas in the west of the model domain, reaching up to 3.52 m under a HEFS. Under all scenarios the greatest water depths in the city centre are located in the low-lying areas adjacent to the north channel, exceeding 2 m in places for a HEFS. Water depths are generally much shallower within the street network, generally < 0.5 m under the current scenario. The maximum total velocity from model snapshots was extracted for each cell within the model domain, for each simulated scenario (Appendix A, Figure A. 3). Under all fluvial scenarios this illustrates patterns of higher peak velocities immediately adjacent to the river channel and in areas where obstacles to flow are minimal, including the rural areas to the west of the city and the plains represented by recreational areas in the city centre. Velocities reduce in the flooded street network where complex topography and narrow flow pathways result in greater bottom friction, and at more distal locations from the river channels as floodwaters lose momentum, becoming increasingly stagnant. The increased volumes of water in the MRFS and HEFS result in an alteration in the wave

velocity. Changes in propagation patterns can result in an increase in velocity in some locations and a decrease in others; on average floodplain velocities increase by 0.07 m/s in the MRFS and 0.10 m/s in the HEFS, with maximum increases of 0.12 and 0.32 m/s respectively.

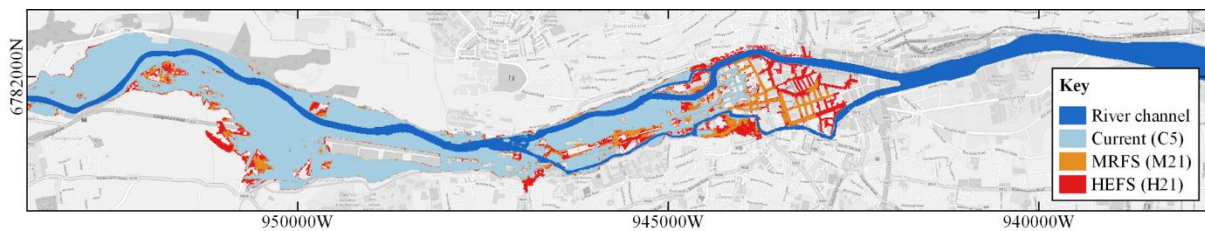


Figure 7: Flood extent resulting from current, medium-range (MRFS) and high-end future scenario (HEFS) 100-year return period fluvial events

4.3 Coastal driven flooding

Coastal mechanisms are also capable of triggering inundation, shown by simulations incorporating MSLR and the exacerbating influence of storm surge residuals on water levels at the downstream boundary. Relative increases in coastal inundation under future climate scenarios, in comparison to the current climate, are much greater than those modelled for fluvial events.

4.3.1 Mean sea level rise

Simulations suggest that existing defences will be capable of preventing flooding under average tides for both a MRFS and HEFS MSLR (Figure 8a), and under spring tidal conditions for a MRFS MSLR; with the exception of minor flooding of low-lying land near the river mouth (Figure 8b). However, 37 ha of inundation is simulated for a HEFS MSLR under spring tides (Figure 8b, Table 3– H2). This is critical as, should such sea-level rise occur, coastal inundation would occur on a bi-monthly basis during each spring tide, regardless of surge conditions. Associated flooding is focused in eastern portions of the city centre, with waters primarily overtopping the south channel and propagating north. Water depths are generally < 0.5 m in areas of inundation, with discrete areas reaching depths of up to 1 m; associated velocities are low (<0.25 m/s).

4.3.2 Storm surges

Consideration must also be made of the potential impact of surge residuals on water levels. When applied to average tides for present-day sea levels, neither the current, MRFS or HEFS peak surge residuals cause flooding (Figure 9). However, a combination of MSLR and either current or HEFS surge residuals can initiate coastal inundation under average tides (Figure 9a and c). Associated water depths are generally shallow (< 0.5 m) and velocities slow, however, these marginally increase under the HEFS surge/HEFS MSLR scenarios (Appendix A, Figure A. 4).

When applied to spring tides, the current peak surge residual causes notable flooding (38 ha) regardless of climate change (Figure 10a, Table 3– C4). Associated water depths are again generally <0.5 m (Appendix A, Figure A. 5a) and velocities <0.25 m/s (Appendix A, Figure A. 6a), although these increase in discrete area to the south of the river. Under a MRFS and HEFS sea level, the co-occurrence of the current peak surge residual with spring tides has the potential to cause significantly greater flooding – 168 ha and 182 ha respectively (Figure 10a, Table 3– M5, H5). Under these scenarios, the

majority of the city centre becomes inundated, and large areas of flooding occur in the Marina industrial area to the south of the river, with significant increases in water depths and velocities (Appendix A, Figure A. 5 and Figure A. 6).

Significant flooding continues under all sea level scenarios for the MRFS reduction in surge height, although this results in a marginal decrease in affected area (Figure 10b). Under a HEFS projection of stronger storm surges, inundation extent increases for all sea level scenarios when compared to the current surge scenario (Figure 10c), with a maximum inundated area of 191 ha resulting from the co-occurrence of a HEFS surge event with a HEFS MSLR (Table 3 – H4). This scenario causes flooding over a greater extent than the current 100-year fluvial flood event, impacting the majority of the city centre and eastern industrial areas (Figure 10c). Water depths and velocities also increase for each associated MSLR scenario (Appendix A, Figure A. 7 and Figure A. 8); with depths of up to 2 m simulated in the city centre.

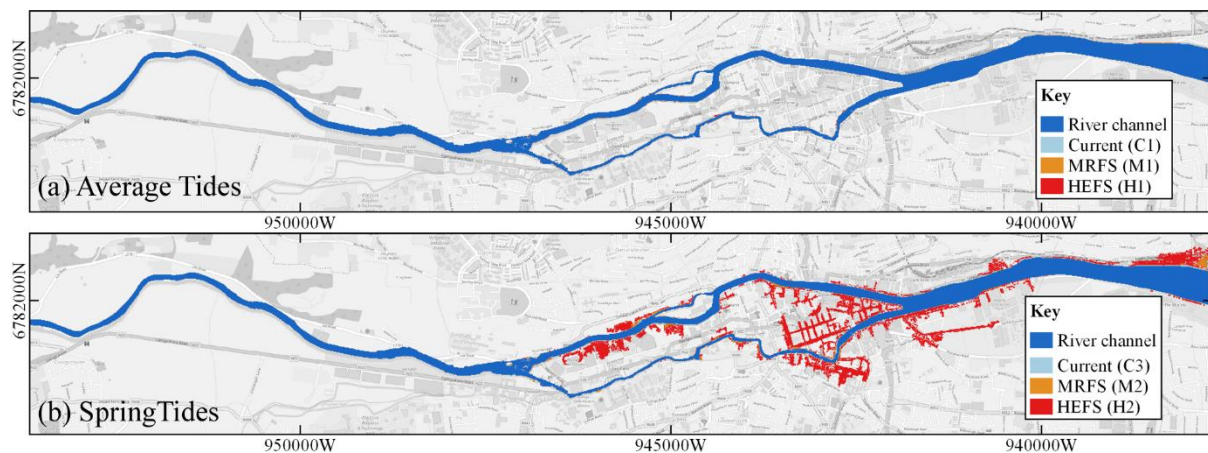


Figure 8: Flood extent resulting from mean sea-level rise under (a) average tides and (b) spring tides

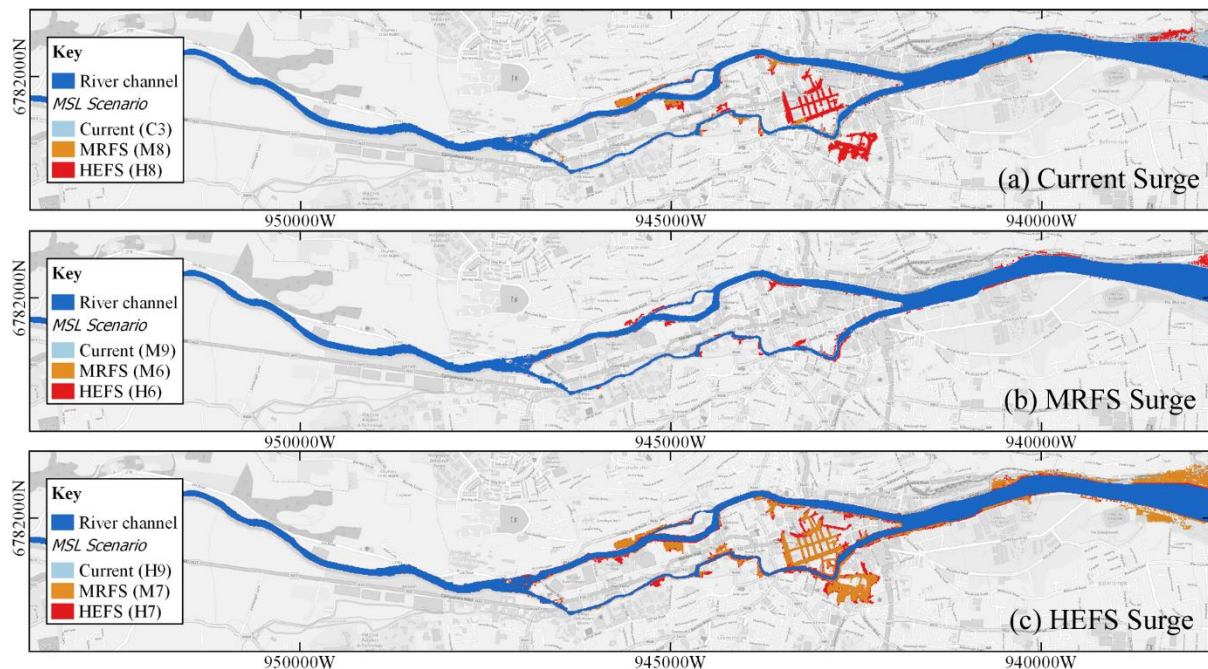


Figure 9: Flood extent resulting from (a) current, (b) medium-range, and (c) high-end surge residuals under current and future mean sea levels and average tides

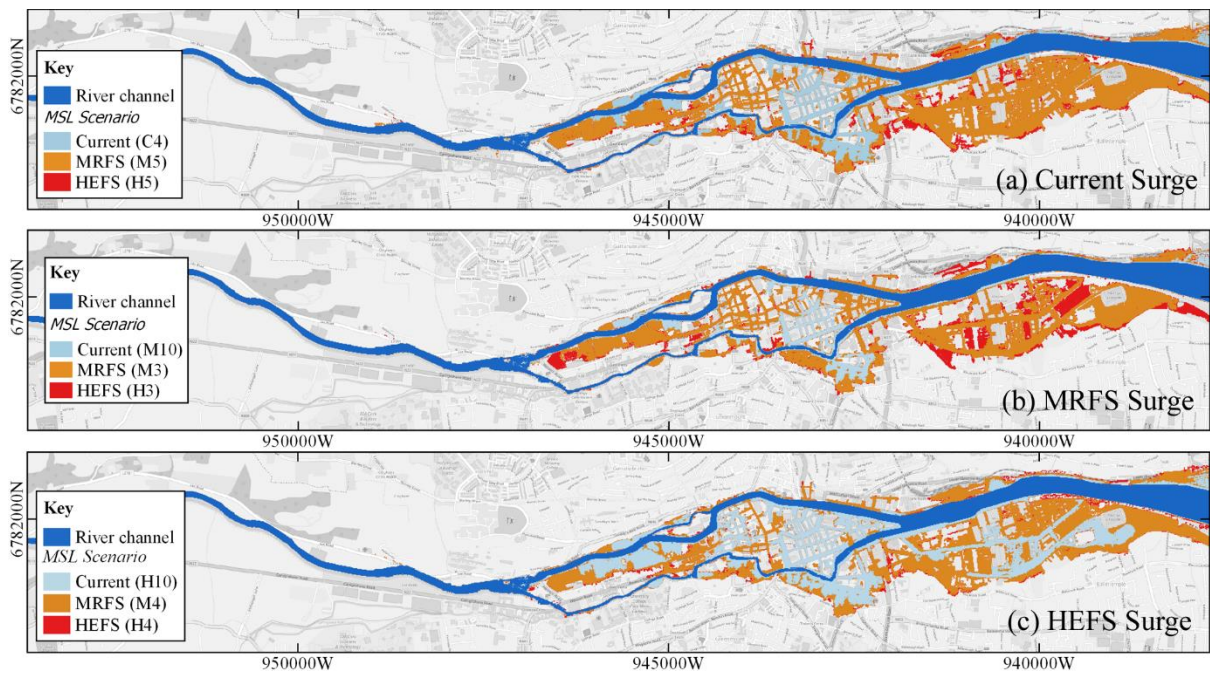


Figure 10: Flood extent resulting from (a) current, (b) medium-range and (c) high-end surge residuals under current and future mean sea levels on spring tides

4.4 Combined fluvial and coastal driven flooding

As well as consideration of autonomous flood drivers, the interaction of sea levels and fluvial flow is an important consideration for effective flood prediction and management (Moftakhari *et al.* 2017).

4.4.1 Non-linear interaction

High coastal water levels are observed to exacerbate fluvial flood extent, with the coincidence of a peak fluvial event with spring rather than average tides increasing city centre inundation (Figure 11, Table 3– C7). This is expected to be a result of high coastal waters restricting fluvial discharge and causing a stacking of water along the riverbanks (Hoitink & Jay 2016). Similarly, simulated medium-range and high-end MSLR, as well as the co-occurrence of surge conditions during a fluvial flood event, have the ability to increase the extent of inundation associated with peak fluvial discharges, under both average and spring tidal conditions (Table 3). Where coastal water levels sufficient to cause inundation independently are combined with peak fluvial flows, flooding becomes exacerbated both by coastal inundation and by the influence of coastal waters on fluvial flows.

Combined fluvial and coastal events are further complicated by the influence of extreme fluvial discharges on coastal inundation. Comparison of inundation extent associated with a HEFS MSL under mean fluvial flows (H2) and under current (H12), MRFS (H39) and HEFS (H24) peak fluvial flows suggests that coastal inundation is reduced by increased river discharges (Appendix A, Figure A. 9). This is expected to be a result of increased volumes and velocities of freshwater inflows restricting the propagation of tides upstream, a process illustrated by Leonardi *et al.* (2015).

4.4.2 Worst-case scenario

Despite a complex relationship between different flood drivers, the most extreme flood events result from the combined impact of high river flows and high coastal water levels. When combined with spring tides under a HEFS MSL, the HEFS peak fluvial event results in 265 ha of inundation (Table 3 – H24). The entirety of the city centre becomes inundated and fluvial flooding of the city downtown is exacerbated by coastal flooding (Figure 12). When combined with a HEFS surge event, 387 ha of inundation is simulated (Table 3– H26). River discharges are insufficient to notably reduce tidal propagation resulting from the associated extreme sea levels, and extensive coastal inundation occurs to the east of the city centre and in urban areas to the south (Figure 12).

Associated water depths and velocity are illustrated in (Appendix A, Figure A. 10 and Figure A. 11). Under this extreme event inundation to the west of the city remains solely fluvial driven and water extent, depth and velocity remains comparable to that resulting exclusively from a HEFS fluvial flood event. To the east of the city centre water depths and velocities are generally comparable to those resulting exclusively from coastal inundation. However, the city centre is impacted by both fluvial and coastal inundation, resulting in an increase in water depths compared to those experienced under autonomous drivers. Water velocities are primarily fluvial driven; however, high coastal water levels have the potential to reduce velocities by reducing the gradient of flow. A reduction in maximum water velocity is observed within the eastern reaches of the Lee channel for the combined future event, when compared to the scenario forced exclusively by a HEFS fluvial discharge. Despite this, water velocities in the city centre floodplains are generally unaffected, with the additional overtopping of waters forced by coastal mechanisms increasing velocities in the eastern reaches of the city centre.

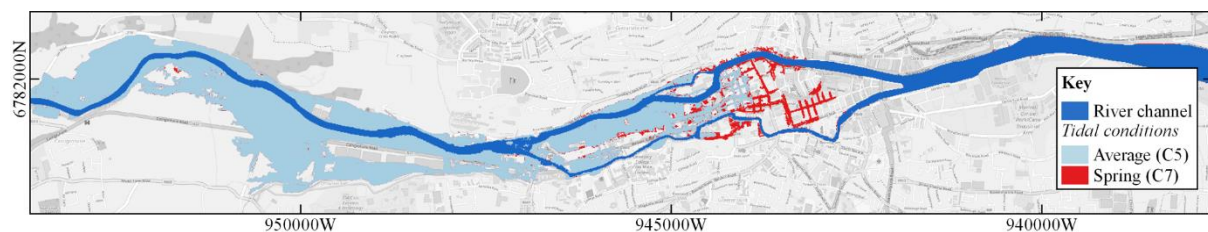


Figure 11: Flood extent resulting from the current 100-year return period fluvial event for average and spring tides

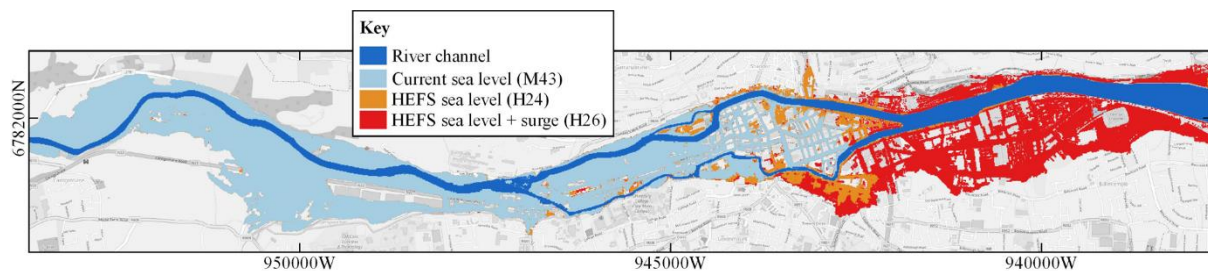


Figure 12: Flood extent resulting from the high-end fluvial flood event on current sea levels, on high-end future sea levels, and on high-end sea levels with a high-end surge residual, all on spring tides

5 CONCLUSIONS

This study aims to understand the conditions under which urban flooding, resulting from various drivers, will occur under current and future climatic conditions, with the overall goal of providing a methodology for comprehensive forecasting and assessment of flooding under changing climates. Cork City is impacted by both fluvial and coastal flood mechanisms, and a combination of thereof, and extensive and costly coastal-fluvial flooding of the city in November 2009 prompted the current investigation. This urban area was used to explore climate driven changes in flood mechanisms, dynamics and extents. Current peak river discharges and coastal water levels affecting the city were determined and 21st Century climate projections utilised to define potential future discharges and water levels. These were employed as model boundary conditions within the MSN_Flood model in order to provide a range of estimates of future inundation.

The main findings of this research are as follows:

- (i) The capability of MSN_Flood to simulate both water elevations and velocity fields makes it a valuable tool for studying coastal flood inundation and for understanding the dynamics of flood wave propagation.
- (ii) The computational efficiency of the nested modelling system enables multiple climate change scenarios to run in a relatively short timeframe, and so facilitates a methodology for accurately stress testing climate change effects on complex coastal-fluvial flooding in urban areas.
- (iii) The range of widely varying inundation patterns generated within this research based on different estimates and combinations of current, medium-range and high-end projections of extreme river flows and sea level indicate that the most pertinent inferences on potential future inundation patterns must be drawn from an ensemble of model simulations.
- (iv) The methodology explored in this research demonstrates the best practice for stress testing climate change effects on flooding. Various drivers of flooding can be analysed separately and jointly so that their individual and combined impacts under changing climate can be determined, and a multivariate climate change analysis allows identification of future flood-prone areas.
- (v) The potential exposure of communities to flooding is a critical task for long term planning and risk assessment. The methodologies utilised within this research can help establish the most effective adaptation plan and as such facilitate decision making in flood defence design and flood risk management.

Due to its robust wetting and drying routine, MSN_Flood is adaptable to any domain, regardless of complexity, and to multi-open boundary problems. As a result, it can be applied to any urban coastal floodplain to aid in climate adaptation. Within this research the model was applied to Cork City and domain specific findings are as follows:

- (i) The MSN_Flood modelling system has been shown capable of accurately resolving the complex hydrodynamics of the domain at scales commensurate with flow features. Inundation in both the upstream rural floodplains and in the downstream network of dense streets was accurately reproduced by the 6 m urban flood model.
- (ii) Under current conditions the fluvial signal is a primary driver of flooding, with extreme fluvial flooding responsible for the greatest inundation (affecting 187 ha). Storm surges are capable

of causing up to 38 ha of coastal inundation in the eastern reaches of the city under mean fluvial conditions.

- (iii) Climate-driven increases in fluvial flows have the potential to increase the inundated area (up to 242 ha) by 30% compared to current fluvial peak conditions, with waters propagating further downtown into the city centre.
- (iv) Climate-driven changes in both MSL and surges could result in a staggering 400% increase in coastal inundation (up to 191 ha) when compared to current climate (38 ha), resulting in inundation over a greater aerial extent than the current extreme fluvial event (187 ha). Although, the extreme future fluvial flows will still generate greater extent of flooding (up to 242 ha), there is a significant shift in contribution towards the coastal mechanism.
- (v) Coastal flooding (unlike fluvial inundation) predominantly affects the eastern reaches of the city and the majority of the city centre, where a significant portion of socio-economic wealth is accumulated. Future coastal flooding will prevail in highly urbanised areas and thus have a major socio-economic impact.
- (vi) Rising mean sea levels have the potential to overwhelm existing defences and inundate parts of the city centre during spring tides, regardless of surge conditions. Without appropriately adapted flood defence systems, coastal inundation could occur on a bi-monthly basis during each spring tide.
- (vii) Increased coastal water levels are shown to impact the conveyance of fluvial flows to the ocean and extreme fluvial discharges to impact the propagation of coastal waters inland, illustrating the requirement for accurate modelling of the dynamics of combined coastal-fluvial systems.
- (viii) For current climate, the most extreme flood events occur due to a combination of peak river flows and high coastal water levels, with 243 ha of inundation resulting from the coincidence of the 100-year return river discharge and peak surge residual on spring tides for current conditions.
- (ix) Climate-driven increases in both fluvial and coastal mechanisms have the potential to cause up to 387 ha of inundation across the model domain for the worst-case scenario coastal-fluvial flood event. This is an increase in inundation by 76% compared to the 2009 flood event. Water depths and velocities, exacerbated by both fluvial and coastal mechanisms, create a significant threat to the populace across the majority of the city.

Overall, this research demonstrates that the adopted methodology can be successfully used to understand the major effects that climate change may have on future flooding.

ACKNOWLEDGEMENTS

The authors would like to thank OPW, Ireland for hydrological data and Dr Stephen Nash for making the MSN_Flood model available.

REFERENCES

- Arns A., Wahl T., Dangendorf S., & Jensen J. 2015 The impact of sea level rise on storm surge water levels in the northern part of the German Bight. *Coastal Engineering*, 96, 118-131.
- Bastola S., Murphy C., & Sweeney J. 2011a The role of hydrological modelling uncertainties in assessments of Irish river catchments. *Advances in Water Resources*, 34, 562-576.
- Bastola S., Murphy C., & Sweeney J. 2011b The sensitivity of fluvial flood risk in Irish catchments to the range of IPCC AR4 climate change scenarios. *Science of the Total Environment*, 409, 5403-5415.
- Bates P. D., Horrit M. S., & Fewtrell T. J. 2010 A simple inertial formulation of the shallow water equations for efficient two-dimensional flood inundation modelling. *Journal of Hydrology*, 33-45.
- Barnard P.L., Erikson L.H., Foxgrover A.C., Finzi Hart J.C., Limber P., O'Neill, A.C., vanOrmond, M., Vitousek S., Wood, N., Hayden M.K., Jones, J.M. 2019 Dynamic food modeling essential to assess the coastal impacts of climate change. *Nature*, 9:4309
- Bradley S., Milne G. A., Teferle, F. N., Bingley R. M., & Orliac, E. J. 2009 Glacial isostatic adjustment of the British Isles: new constraints from GPS measurements of crustal motion. *Geophysical Journal International*, 178, 14-22.
- Brown J., Souza A. J., & Wolf J. 2010 Surge modelling in the eastern Irish Sea: present and future storm impact. *Ocean Dynamics*, 60, 227-236.
- Chiverrell R. C., & Thomas G. S. 2010 Extent and timing of the Last Glacial Maximum (LGM) in Britain and Ireland: a review. *Journal of Quaternary Science*, 25, 535-549.
- Comer J., Olbert A. I., Nash S., & Hartnett M. 2017 Development of high-resolution multi-scale modelling system for simulation of coastal-fluvial urban flooding. *Natural Hazards and Earth System Sciences*, 17, 205-224.
- Dunne S., Hanafin, J., Lynch, P., McGrath, R., Nishimura, E., Nolan, P., et al. 2008 *Ireland in a Warmer World, Scientific Predictions of the Irish Climate in the Twenty-First Century*. (R. McGrath and P. Lynch, eds.): Community Climate Change Consortium for Ireland (C4I).
- Eichler T. P., Gaggini, N., & Pan, Z. 2013 Impacts of global warming on Northern Hemisphere winter storm tracks in the CMIP5 model suite. *Journal of Geophysical Research: Atmospheres*, 118(10), 3919-3932.
- Fettweis X., Franco, B., Tedesco, M., van Angelen, J. H., Lenaerts, J. T., van den Broeke, M. R., et al. 2013 Estimating the Greenland ice sheet surface mass balance contribution to future sea level rise using the regional atmospheric climate model MAR. *The Cryosphere*, 7, 469-489.
- Fortunato A., & Mazzola, O. M. 2014 Selection of the Optimal Design Rainfall Return Period for Urban Drainage Systems. *Procedia Engineering*, 89, 742-749.

- Gallagher S., Gleeson, E., Tiron, R., McGrath, R., & Dias, F. 2016 Wave climate projections for Ireland for the end of the 21st century including analysis of the the EC-Earth winds over the North Atlantic Ocean. *International Journal of Climatology*, 36, 4592-4607.
- Gill A. E. 1982 *Atmosphere-Ocean Dynamics*. London: Academic Press.
- Green J. 2010 Ocean tides and resonance. *Ocean Dynamics*, 60, 1243-1253.
- Haarsma R. J., Hazeleger, W., Severijns, C., de Vries, H., Sterl, A., Bintanja, R., et al. 2013 More hurricanes to hit western Europe due to global warming. *Geophysical Research Letters*, 40, 1783 - 1788.
- Halcrow 2009 *Lee CFRAMS Hydrology Report*. Cork: Halcrow Group Ireland.
- Halcrow 2014 *Lee CFRAMS Catchment Flood Risk Management Plan*. Dublin: Halcrow Group Ireland.
- Hall J., Arheimer B., Borga, M., Brazdil, R., Claps, P., Kiss, A., et al. 2014 Understanding flood regime changes in Europe: a state-of-the-art assessment. *Hydrology and Earth System Science*, 18(7), 2735-2772.
- Hallegatte S., Green, C., & Nicholls, R. J. 2013 Future flood losses in major coastal cities. *Nature Climate Change*, 802-806.
- Hewitt R. L., & Lees-Spalding, I. J. 1982 *The Maximilian and Silk Cut Nautical Almanac*. The Macmillan Press Ltd.
- Hoitink A. J., & Jay, D. A. 2016 Tidal river dynamics: Implications for deltas. *Reviews of Geophysics*, 54(1), 240-272.
- ICHARM 2009 *Global Trends in Water-Related Disasters: an insight for policymakers*. Paris: International Centre for Water Hazard and Risk Management (UNESCO).
- IPCC 2013 *Climate Change 2013: The Physical Science Basis. Working Group I Contribution to the Fifth Assessment Report of the Intergovernmental Panel on Climate Change*. [Stocker, T., Qin, D., Plattner, G-K., Tignor, M., Allen, S., Boschung, J., Nauels, A. Xia, Y., Bex, V. & Midgley, P. (eds)]. Cambridge: Cambridge University Press.
- Jevrejeva S., Grinsted, A., & Moore J. C. 2014 Upper limit of sea level projections by 2100. *Environmental Research Letters*, 9, 104008.
- Joint Research Centre 2014 *Climate Impacts in Europe, The JRC PESERA II Project*. Luxembourg: Publications Office of the European Union.
- Koppel T. 2007 *Ebb and Flow: Tides and Life on Our Once and Future Planet*. Dundum.
- Kundzewicz Z. W. 2012 *Changes in flood risk in Europe*. Wallingford: IAHS Press.
- Lehner B., Doll, P., Alcamo, J., Henrichs, T., & Kaspar, F. 2006 Estimating the impact of global change on flood and drought risks in Europe: a continental integrated analysis. *Climate Change*, 75, 273-299.

- Leonardi N., Kolker, A. S., & Fagherazzi, S. 2015 Interplay between river discharge and tides in a delta distributary. *Advances in Water Resources*, 80, 69-78.
- Levermann A., Winkelmann, R., Nowicki, S., Fastook, J. L., Frieler, K., Greve, R., et al. 2014 Projecting Antarctic ice discharge using response functions from SeaRISE ice-sheet models. *Earth System Dynamics*, 5, 27-293.
- Marzeion B., Jarosch, A. H., & Hofer, M. 2012 Past and future sea-level change from the surface mass balance of glaciers. *The Cryosphere*, 6, 1295-1322.
- McGranahan G., Balk, D., & Anderson, B. 2007 The rising tide: assessing the risks of climate change and human settlements in low elevation coastal zones. *Environment and urbanization*, 19, 17-37.
- Merkens J.-L., Reimann L., Hinkel J. & Vafeidis A. T. 2016 Gridded population projections for the coastal zone under the Shared Socioeconomic Pathways. *Global Planet. Change* **145**, 57–66 (2016)
- Moftakhari H. R., Salvadori G., AghaKouchak A., Sanders, B. F., & Matthew, R. A. 2017 Compounding effects of sea level rise and fluvial flooding. *Proceedings of the National Academy of Sciences of the United States of America*, 114(37), 9785-9790.
- Murphy C. (2013). Chapter 10: Climate change and catchment hydrology. In E. Gleeson, R. McGrath, & M. Treanor (Eds.), *Ireland's Climate: the road ahead* (pp. 63-69). Dublin: Met Eireann.
- Murphy C., & Charlton R. 2008 Climate Change and Water Resources. In J. Sweeney (Ed.), *Climate Change: Refining the Impacts* (pp. 39-72). Wexford: Environmental Protection Agency.
- Murphy C., Cunnane C., Das, S. & Mandal, U. 2014 *Flood Studies Update Technical Research Report Volume II: Flood Frequency Estimation*. Office of Public Works.
- Olbert A. I., Hartnett, M. Comer J., & Nash S. 2015 Mechanisms of flooding in Cork City. *Irish National Hydrology Conference*. Athlone: National Hydrology Conference.
- Olbert A., & Hartnett M. 2010 Storms and surges in Irish coastal waters. *Ocean Modelling*, 34, 50-62.
- Olbert A., Comer J., Nash S., & Hartnett M. 2017 High-resolution multi-scale modelling of coastal flooding due to tides, storm surges and river inflows. A Cork City Example. *Coastal Engineering*, 121, 278-296.
- Olbert A., Dabrowski T., Nash S., & Hartnett M. 2012 Regional modelling of the 21st century climate changes in the Irish Sea. *Continental Shelf Research*, 41, 48-60.
- Olbert A., Nash S., Cunnane C., & Hartnett M. 2013 Tide-surge interactions and their effects on total sea levels in Irish coastal waters. *Ocean Dynamics*, 63(6), 599-614.
- O'Neill A.C., Erikson L.C., Barnard P.L., Limber P.W., Vitousek, S., Warrick, J.A., Foxgrover, A.C., Lovering, J. 2018 Projected 21st century coastal flooding in the Southern California Bight. Part 1: Development of the third generation CoSMoS model. *Journal of Marine Science and Engineering*, 6, 59.

- OPW 2015 *Climate Change Sectoral Adaptation Plan, Flood Risk Management (2015-2019)*. Office of Public Works.
- Parry M., Arnell M., Berry, P., Dodman, D., Fankhauser S., Hope C., et al. 2009 *Assessing the costs of adaptation to climate change: A review of the UNFCCC and other recent estimates*. London: International Institute for Environment and Development and Grantham Institute for Climate Change.
- Pelling H. E., & Mattias Green J. A. 2014 Impact of flood defences and sea-level rise on the European Shelf tidal regime. *Continental Shelf Research*, 85, 96-105.
- Pickering M. D., Wells N. C., Horsburgh K. J., & Green J. A. 2012 The impact of future sea-level rise on the European Shelf tides. *Continental Shelf Research*, 35, 1-15.
- Purvis M. J., Bates P. D., & Hayes C. M. 2008 A probabilistic methodology to estimate future coastal flood risk due to sea level rise. *Coastal Engineering*, 1062-1073.
- Shennan I., Milne G., & Bradley S. 2012 Late Holocene vertical land motion and relative sea-level changes: lessons from the British Isles. *Journal of Quaternary Science*, 27(1), 64-70.
- Steele-Dunne S., Lynch P., McGrath R., Semmier T., Wang, S., Hanafin, J., et al. 2007 The impacts of climate change on hydrology in Ireland. *Journal of Hydrology*, 356, 28-45.
- Teng J., Jakeman A. J., Vaze J., Croke B. F., Dutta D., & Kim S. 2017 Flood inundation modelling: A review of methods, recent advances and uncertainty analysis. *Environmental Modelling & Software*, 90, 201-216.
- Veijalainen N., Lotsari E., Alho P., Vehvilainen B., & Kayhko J. 2010 National scale assessment of climate change impacts on flooding in Finland. *Journal of Hydrology*, 391(3-4), 333-350.
- Vousdoukas M. I., Mentaschi L., Voukouvalas E., Verlaan M., & Feyen L. 2017 Extreme sea levels on the rise along Europe's coasts. *Earth's Future*, 5, 304-323.
- Wahl T., Jain S., Bender J., Meyers S. D., & Luther M. E. 2015 Increasing risk of compound flooding from storm surge and rainfall for major US cities. *Nature Climate Change*, 5, 1093-1097.
- Wang S., McGrath R., Hanafin J., Lynch P., Semmler T., & Nolan P. 2008 The impact of climate change on storm surges over Irish Waters. *Ocean Modelling*, 25, 83-94.
- Wells N. 1997 *The Atmosphere and Ocean*. Chichester: Wiley.
- Woodworth P. L. 2010 A survey of recent changes in the main components of the ocean tide. *Continental Shelf Research*, 30, 1680-1691.
- Woth K., Weisse R., & von Storch H. 2006 Climate change and North Sea storm surge extremes: an ensemble study of storm surge extremes expected in a change projected by four different regional climate models. *Ocean Dynamics*, 3-15, 56.

Table 1: Summary of predictions of impacts on fluvial and coastal flood mechanisms at global scales and local scales relative to Cork City for the 21st Century

Study	Region/ Catchment	Projection Period	Future Climate Scenario		FLUVIAL MECHANISMS					COASTAL MECHANISMS			
					Δ Winter Stream Flows (%)	Δ Peak Flow (%)	Δ Flood Peak of Given Return Period (%)				Δ MSL (m)	Δ Land Elevation (mm/year)	Δ M2 tidal amplitude (m)
						5	25	50	100				
Steele-Dunne, et al., 2017	Blackwater & Bandon	2021-2060	SRES A1B	MRFS	Up to 20% increase								
Halcrow, 2009	Lee & Cork Harbour	2100	Ensemble[†]	MRFS		20				0.5	-0.5		
OPW, 2015				HEFS		30					1.0 ‡	-0.5	
Bastola, et al., 2011b	Blackwater	2071-2100	Ensemble[§]	Lower 5%		12.7	12.6	13.2	13.8				
				Median		16	15.6	15.7	15.8				
				Upper 95%		31.3	36.3	39.1	42.1				
IPCC, 2013	Global Mean Sea Level	2081-2100		RCP2.6[¶]	LEFS					0.40 (0.26-0.55)			
				RCP4.5	MRFS					0.47 (0.32-0.63)			
				RCP6.0	M-HRFS					0.48 (0.33-0.63)			
				RCP8.5	HEFS					0.63 (0.45-0.82)			
Olbert, et al., 2012	Irish Sea	2100	SRES A1B[◇]	MRFS					0.47				
Jevrejeva, et al., 2014	Global Mean Sea Level	2100	RCP8.5	HEFS					1.8				
Shennan, et al., 2012	Cork Area	n/a		n/a ^Δ							-0.4		
Pickering, et al., 2012	Cork Harbour	n/a	2 m SLR	HEFS								-1	
Wang, et al., 2008	Cork Harbour	2031-2060	SRES A1B	MRFS									-17.6

† Based on a range of contemporaneous sources as detailed in Halcrow (2009).

‡ Includes a 0.1 m increase in surge height.

§ 17 GCMs forced with three SRES emission scenarios (A1B, A2 and B1) from the IPCC Fourth Assessment Report (AR4). A1B is as described above, A2 is a scenario of a divided world with regionally orientated development and no one policy on emissions, B1 scenario represents an integrated and ecologically friendly future with emphasis on environmental sustainability.

¶ Representative Concentration Pathways (RCPs) represent the four greenhouse gas concentration trajectories adopted by the IPCC for its Fifth Assessment Report (AR5). RCP2.6 assumes GHG emissions peak between 2010 and 2020 then decline, RCP4.5 assumes emissions peak ~2040 then decline, RCP6.0 assumes emissions peak ~2080 then decline, and RCP8.5 assume emissions continue to rise throughout the 21st Century.

◇ Special Report on Emissions Scenario (SRES) A1B adopted by the IPCC for its Third Assessment Report (TAR) is characterised by a global balanced emphasis on all energy sources and provides a mid-range future climate scenario (as opposed to a fossil intensive scenario or emphasis on non-fossil energy sources).

Δ Based on estimated Late Holocene land motions, future projections not available.

Table 2. Model Boundary Conditions

Mechanism	Current	MRFS	HEFS
Fluvial			
Mean flow	75.0 m ³ /s		
Peak flow	512.3 m ³ /s	+15.8% †	+42.1% †
Coastal			
Mean HWT		1.40 m above MSL	
Max. HWT		2.23 m above MSL	
MSL + Subsidence	0.00 m	+0.50 m ‡	+0.63 m ‡
Peak Surge Residual	0.97 m	-17.76% §	+15% ¶

† Bastola, et al., 2011b
‡ IPCC, 2013, Olbert, et al., 2012 & Shennan, et al., 2012
§ Wang, et al., 2008
¶ Arbitrary

Table 3: Simulated inundation characteristics for current and future flood scenarios

Storm Surge Scenario	Mean Sea level Scenario	Fluvial Discharge Scenario											
		Baseflow Only - 75 m ³ /s			Current Peak - 512 m ³ /s			MRFS Peak - 593 m ³ /s			HEFS Peak - 728 m ³ /s		
		ID	Inundated area (ha)	Volume (litres)	ID	Inundated area (ha)	Volume (litres)	ID	Inundated area (ha)	Volume (litres)	ID	Inundated area (ha)	Volume (litres)
Average tides													
No surge	Current - 1.4 m	<i>C1</i>	-	-	<i>C5</i>	187	2,671	<i>M21</i>	208	3,073	<i>H21</i>	242	3,844
	MRFS - 1.9 m	<i>M1</i>	-	-	<i>M11</i>	194	2,740	<i>M23</i>	219	3,163	<i>M35</i>	247	3,924
	HEFS - 2.03 m	<i>H1</i>	-	-	<i>H11</i>	193	2,743	<i>H35</i> †	215	3,135	<i>H23</i>	244	3,887
Current (0.97 m)	Current - 2.37 m	<i>C2</i>	6.3	21	<i>C6</i>	201	2,806	<i>M22</i>	225	3,257	<i>H22</i> †	242	3,863
	MRFS - 2.87 m	<i>M8</i>	10	79	<i>M18</i>	220	2,965	<i>M30</i>	237	3,359	<i>M36</i>	263	4,149
	HEFS - 3 m	<i>H8</i>	25	149	<i>H18</i>	229	3,030	<i>H36</i> †	238	3,351	<i>H30</i> †	261	4,064
MRFS (0.80 m)	Current - 2.2 m	<i>M9</i>	2.4	33	<i>M19</i>	196	2,770	<i>M31</i>	222	3,212	<i>H31</i>	244	3,899
	MRFS - 2.7 m	<i>M6</i>	5.7	59	<i>M16</i>	217	2,939	<i>M28</i>	230	3,307	<i>M37</i>	259	4,165
	HEFS - 2.83 m	<i>H6</i>	8.7	70	<i>H16</i>	217	2,942	<i>H37</i>	236	3,383	<i>H28</i>	261	4,130
HEFS (1.12 m)	Current - 2.52 m	<i>H9</i>	3.5	45	<i>H19</i>	205	2,847	<i>M33</i>	226	3,276	<i>H33</i> †	243	3,882
	MRFS - 3.02 m	<i>M7</i>	29	163	<i>M17</i>	239	3,124	<i>M29</i>	250	3,483	<i>M38</i> †	262	7,081
	HEFS - 3.15 m	<i>H7</i>	36	209	<i>H17</i>	242	3,156	<i>H38</i> †	246	3,416	<i>H29</i> †	270	4,138
Spring tides													
No surge	Current - 2.23 m	<i>C3</i>	2.8	223	<i>C7</i>	197	2,777	<i>M44</i>	220	3,187	<i>M43</i> †	241	3,832
	MRFS - 2.73 m	<i>M2</i>	5.8	61	<i>M12</i>	208	2,879	<i>M24</i>	236	3,382	<i>M39</i>	255	4,057
	HEFS - 2.86 m	<i>H2</i>	37	149	<i>H12</i>	229	3,037	<i>H39</i>	234	3,349	<i>H24</i>	265	4,222
Current (0.97 m)	Current - 3.2 m	<i>C4</i>	37	223	<i>C8</i>	243	3,162	<i>H43</i>	259	3,549	<i>H44</i>	287	3,549
	MRFS - 3.7 m	<i>M5</i>	168	2036	<i>M15</i>	323	4,153	<i>M27</i>	337	4,569	<i>M40</i>	356	5,328
	HEFS - 3.83 m	<i>H5</i>	182	2318	<i>H15</i>	342	4,719	<i>H40</i>	356	5,163	<i>H27</i>	371	5,842
MRFS (0.80 m)	Current - 3.03 m	<i>M10</i>	29	163	<i>M20</i>	227	3,029	<i>M32</i>	251	3,525	<i>H32</i>	284	4,247
	MRFS - 3.53 m	<i>M3</i>	146	1643	<i>M13</i>	295	3,666	<i>M25</i>	313	4,136	<i>M41</i> †	324	4,675
	HEFS - 3.66 m	<i>H3</i>	147	1274	<i>H13</i>	318	4,035	<i>H41</i> †	325	4,332	<i>H25</i> †	344	5,028
HEFS (1.12 m)	Current - 3.35 m	<i>H10</i>	92	570	<i>H20</i>	261	3,284	<i>M34</i>	279	3,728	<i>H34</i> †	293	4,312
	MRFS - 3.85 m	<i>M4</i>	182	2344	<i>M14</i>	352	4,817	<i>M26</i> †	355	5,169	<i>M42</i> †	377	5,985
	HEFS - 3.98 m	<i>H4</i>	191	2652	<i>H14</i>	356	5,343	<i>H42</i> †	364	5,652	<i>H26</i>	387	6,448

† Model became unstable with 30 second timestep, reduced to 15 seconds

Table 4: Water depths in model domain for current and future fluvial flood scenarios

	Current	MRFS	HEFS
Maximum depth: total inundated area	3.24 m	3.35 m	3.52 m
Maximum depth: <i>city centre</i>	1.66 m	1.89 m	2.32 m
Depth range in majority of inundated streets: <i>west of Grattan Street</i>	<0.5 m	0.5-1.0 m	1.0-1.5 m
Depth range in majority of inundated streets: <i>east of Grattan Street</i>	0 m	<0.5 m	< 1.0 m

Appendix A

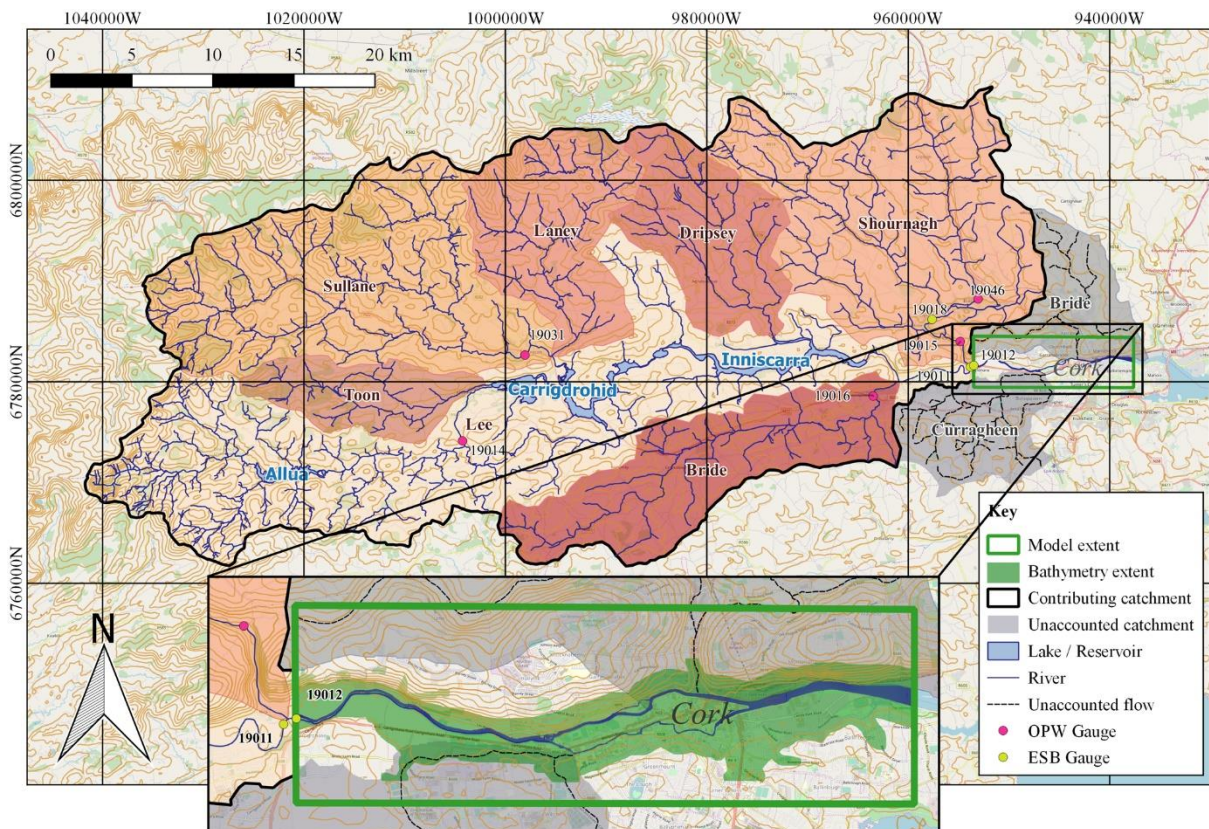


Figure A. 1: Contributing catchment to the CG06 western boundary and (inset) extent of model bathymetry

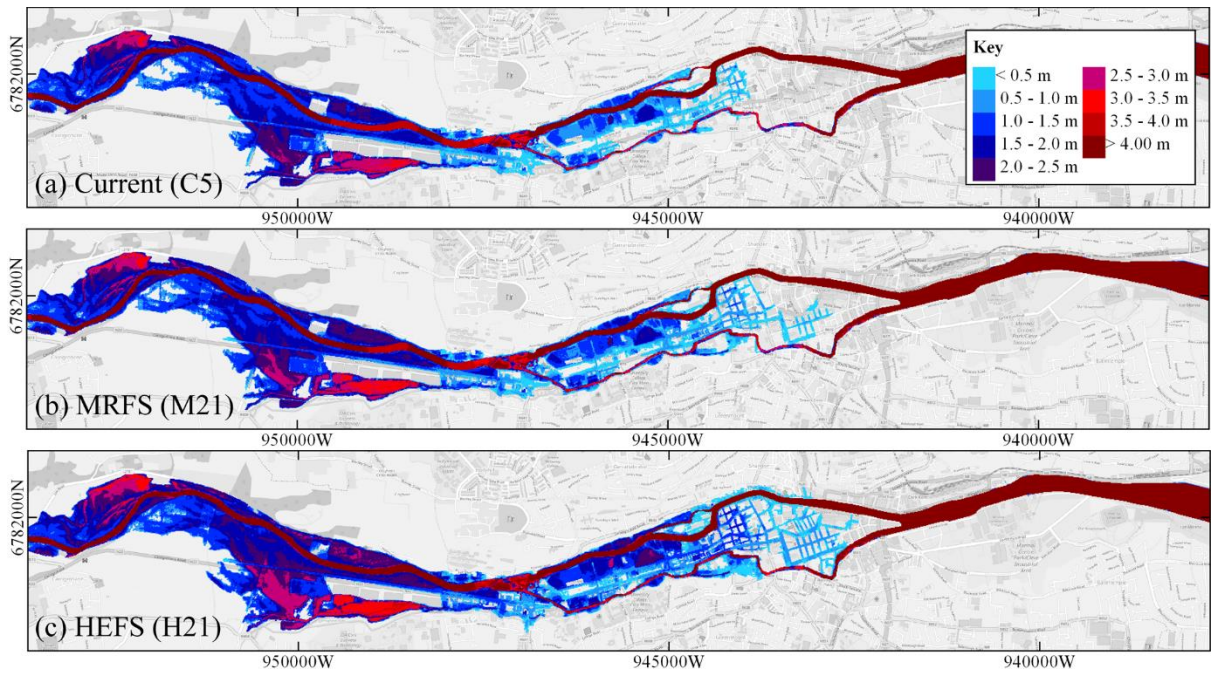


Figure A. 2: Maximum water depths under (a) current, (b) medium-range, and (c) high-end fluvial flood scenarios

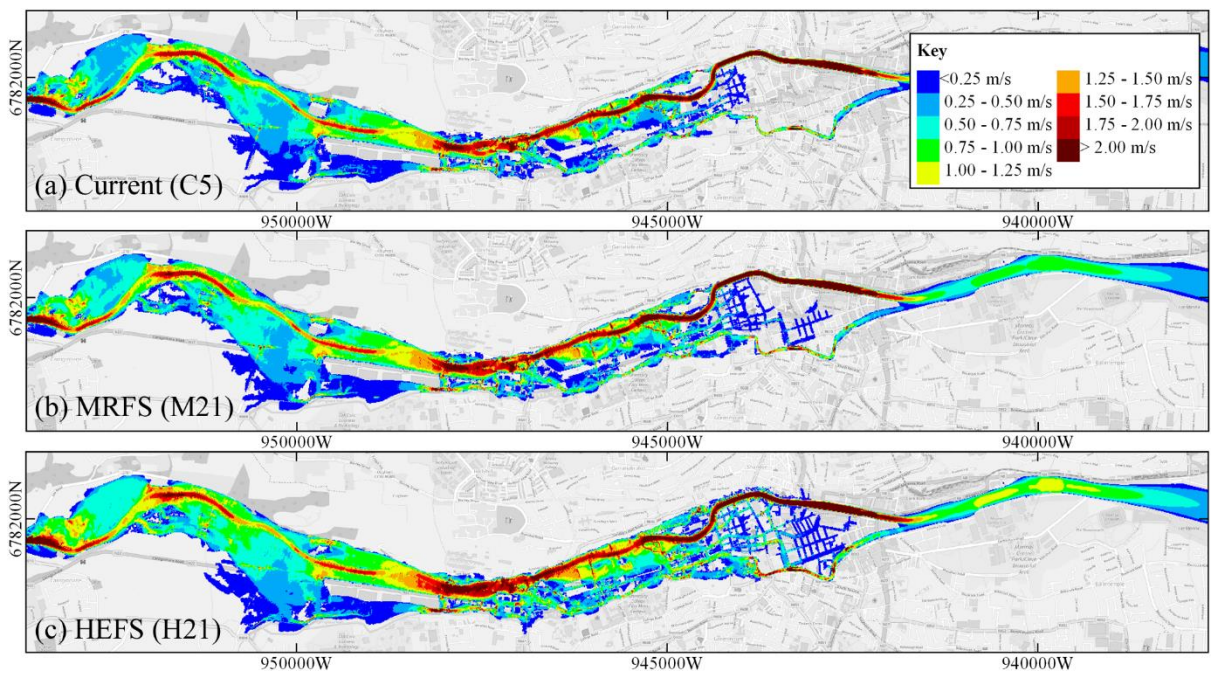


Figure A. 3: Maximum water velocities under (a) current, (b) medium-range, and (c) high-end fluvial flood scenarios

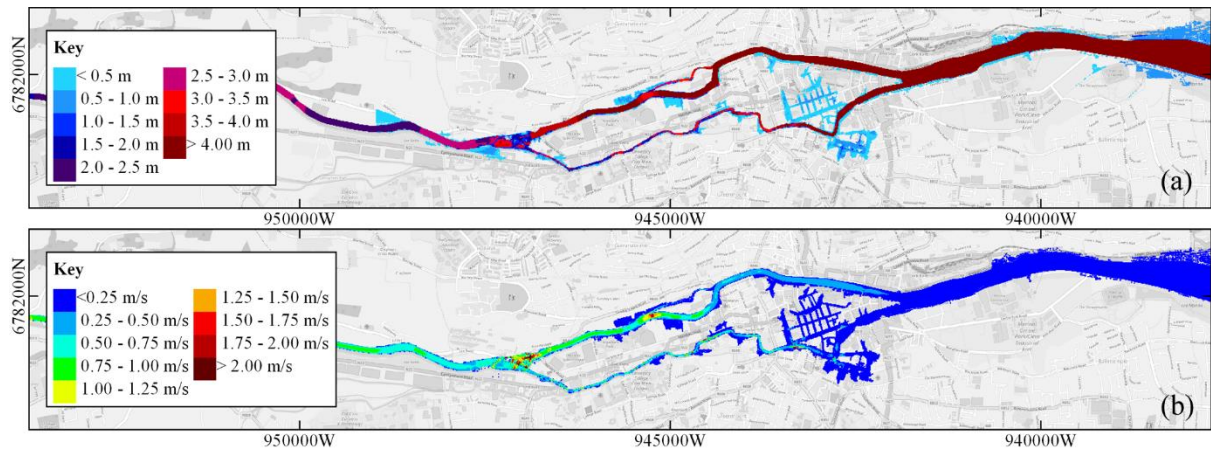


Figure A. 4: Floodwater (a) depths and (b) velocities resulting from a high-end surge residuals under high-end mean sea levels on average tides (H7)

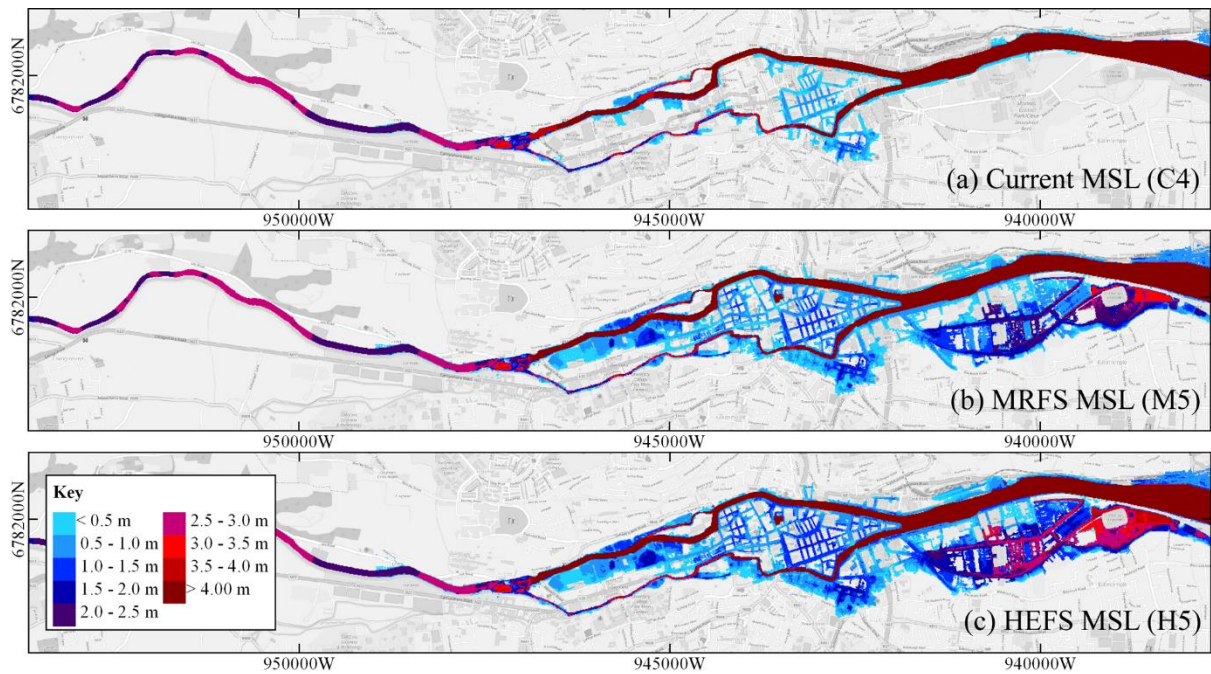


Figure A. 5: Maximum water depths under current surge conditions for (a) current, (b) medium-range, and (c) high-end sea levels

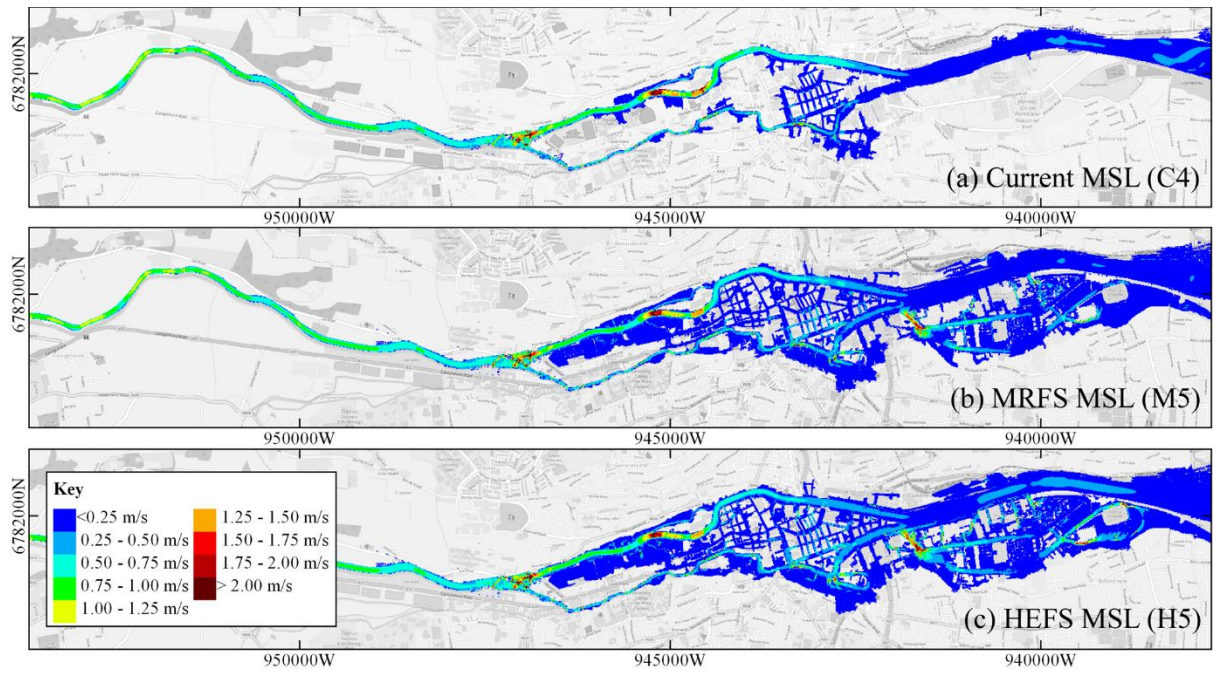


Figure A. 6: Maximum water velocities under current surge conditions for (a) current, (b) medium-range, and (c) high-end sea levels

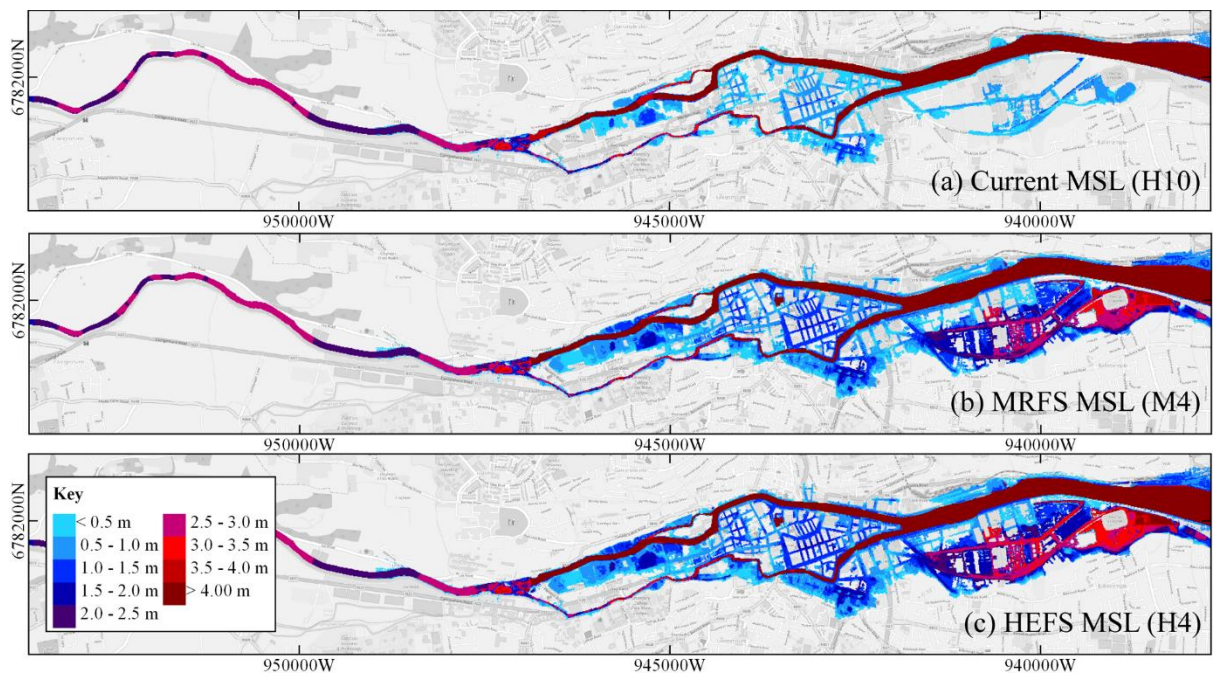


Figure A. 7: Maximum water depths under high-end surge conditions for (a) current, (b) medium-range, and (c) high-end sea levels

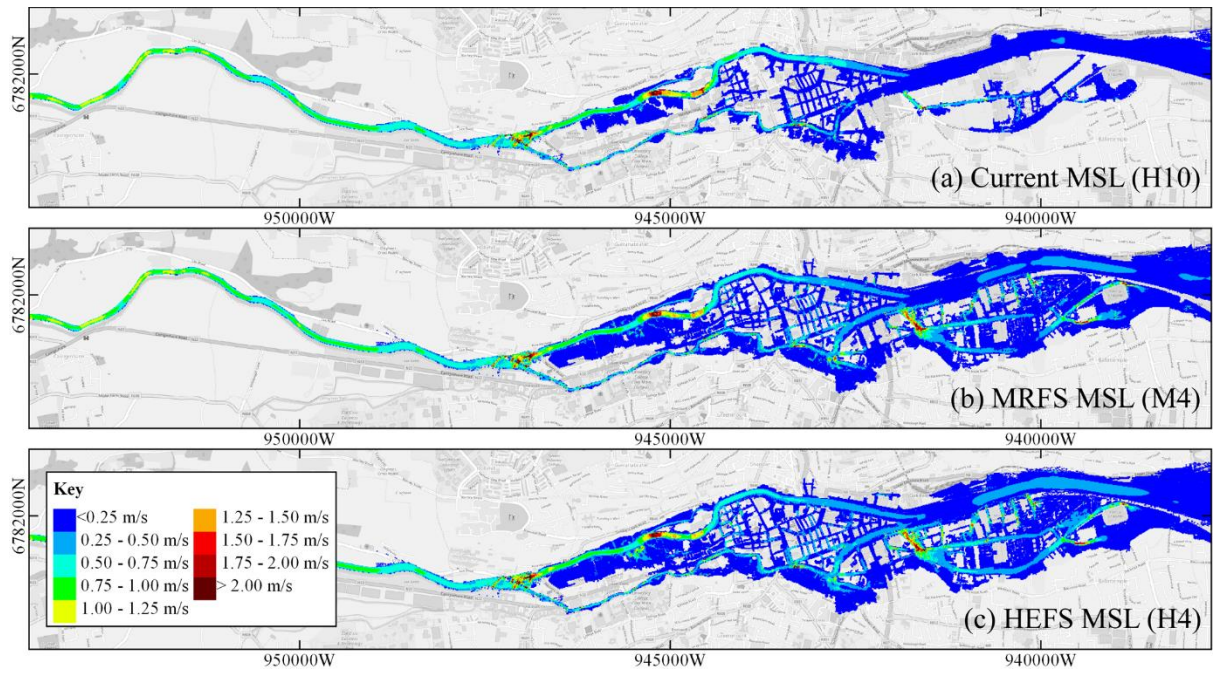


Figure A. 8: Maximum water velocities under high-end surge conditions for (a) current, (b) medium-range, and (c) high-end sea levels

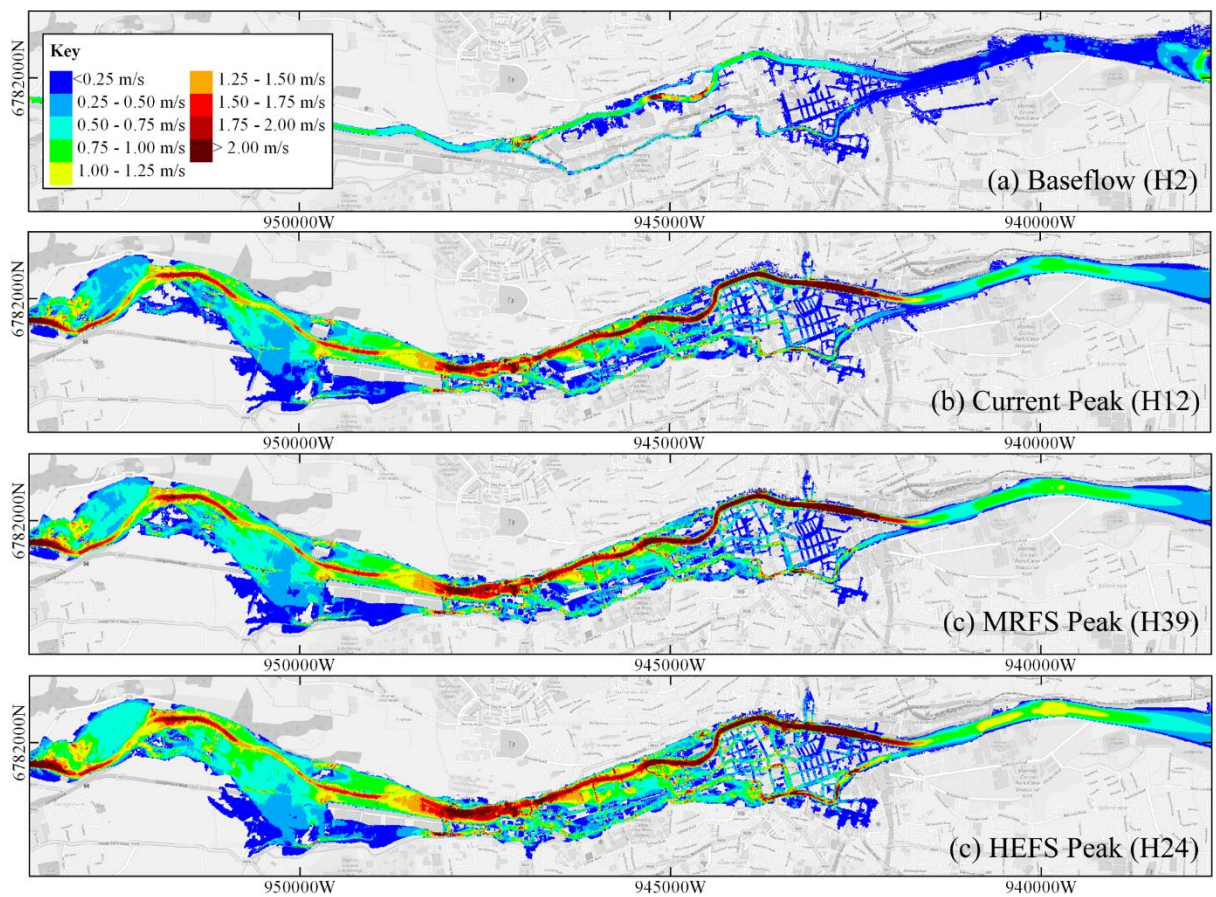


Figure A. 9: Maximum water velocities under high-end future sea levels for (a) mean fluvial conditions, and (b) current, (c) medium-range, and (d) high-end fluvial flood scenarios

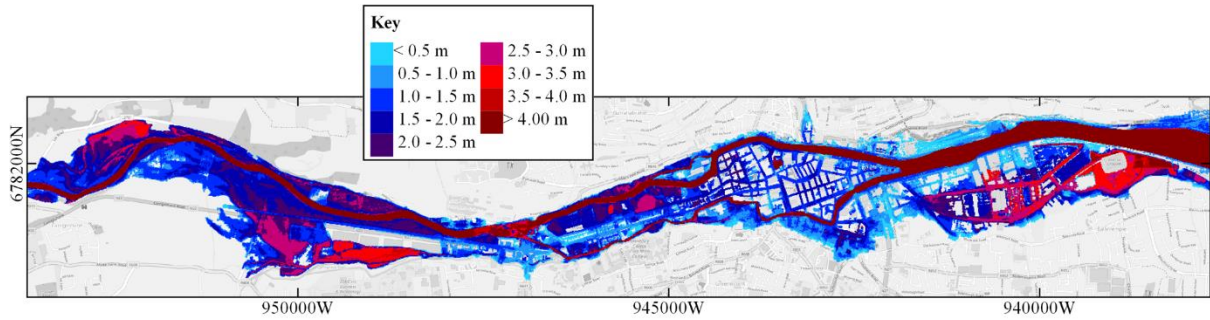


Figure A. 10: Maximum water depths under combined high-end fluvial discharges and coastal water levels

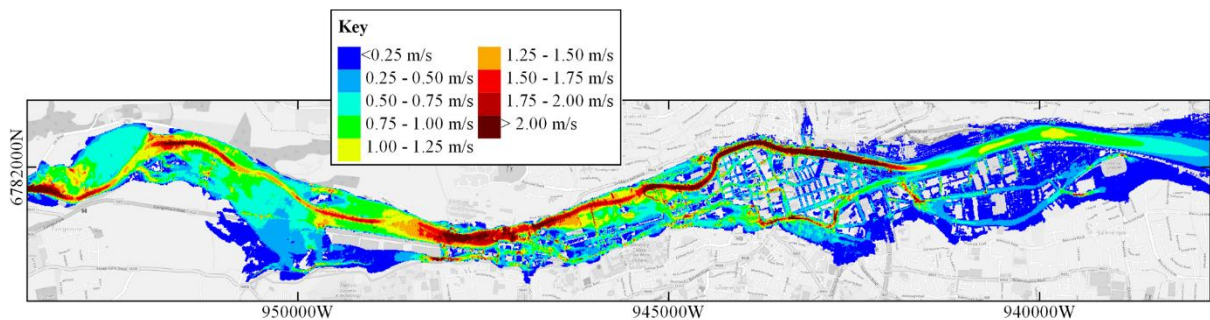


Figure A. 11: Maximum water velocities under combined high-end fluvial discharges and coastal water levels

List of Figures

Figure 13: Study area, with four-level nesting structure of Cork Harbour and Cork City nested models (after Comer, et al., 2017)

Figure 14: (a) 100-year return period synthetic hydrograph; and (b) extracted model inputs for average and peak flow conditions, under current and future climate scenarios

Figure 15: (a) Synthetic mean tidal signals for current, medium range (MRFS) and high-end (HEFS) future scenario mean sea level rise; (b) synthetic maximum tidal signal for current, MRFS and HEFS mean sea level rise; (c) synthetic mean tidal signal with maximum surge residual for current, MRFS and HEFS surge signals. and (d) synthetic maximum tidal signal with maximum surge residual for current, MRFS and HEFS surge signals.

Figure 16: Model boundary conditions for model validation, defined by (a) River Lee flow data (gauge 19011) and (b) tidal water levels (Tivoli tidal gauge) recorded during the November 2009 flood event

Figure 17: Comparison of OPW post-event mapping and modelled inundation extent for the November 2009 flood event

Figure 18: Correlation of modelled and observed water elevations at survey locations

Figure 19: Flood extent resulting from current, medium-range (MRFS) and high-end future scenario (HEFS) 100-year return period fluvial events

Figure 20: Flood extent resulting from mean sea-level rise under (a) average tides and (b) spring tides

Figure 21: Flood extent resulting from (a) current, (b) medium-range, and (c) high-end surge residuals under current and future mean sea levels and average tides

Figure 22: Flood extent resulting from (a) current, (b) medium-range and (c) high-end surge residuals under current and future mean sea levels on spring tides

Figure 23: Flood extent resulting from the current 100-year return period fluvial event for average and spring tides

Figure 24: Flood extent resulting from the high-end fluvial flood event on current sea levels, on high-end future sea levels, and on high-end sea levels with a high-end surge residual, all on spring tides

Appendix A

Figure A. 12: Contributing catchment to the CG06 western boundary and (inset) extent of model bathymetry

Figure A. 13: Maximum water depths under (a) current, (b) medium-range, and (c) high-end fluvial flood scenarios

Figure A. 14: Maximum water velocities under (a) current, (b) medium-range, and (c) high-end fluvial flood scenarios

Figure A. 15: Floodwater (a) depths and (b) velocities resulting from a high-end surge residuals under high-end mean sea levels on average tides (H7)

Figure A. 16: Maximum water depths under current surge conditions for (a) current, (b) medium-range, and (c) high-end sea levels

Figure A. 17: Maximum water velocities under current surge conditions for (a) current, (b) medium-range, and (c) high-end sea levels

Figure A. 18: Maximum water depths under high-end surge conditions for (a) current, (b) medium-range, and (c) high-end sea levels

Figure A. 19: Maximum water velocities under high-end surge conditions for (a) current, (b) medium-range, and (c) high-end sea levels

Figure A. 20: Maximum water velocities under high-end future sea levels for (a) mean fluvial conditions, and (b) current, (c) medium-range, and (d) high-end fluvial flood scenarios

Figure A. 21: Maximum water depths under combined high-end fluvial discharges and coastal water levels

Figure A. 22: Maximum water velocities under combined high-end fluvial discharges and coastal water levels